Dual Emissive Zn(II) Naphthalocyanines: Synthesis, Structural and Photophysical Characterization with Theory-Supported Insights towards Soluble Coordination Compounds with Visible and Near-Infrared Emission

Sidharth Thulaseedharan Nair Sailaja 1,2 , Iván Maisuls 1,2, Alexander Hepp 1 , Dana Brünink 3,
Nikos L. Doltsinis 3 , Andreas Faust 4,5, Sven Hermann 4,5 and Cristian A. Strassert 1,2,*
1 Institut für Anorganische und Analytische Chemie, Universität Münster, Corrensstraße 28/30,
48149 Münster, Germany; maisuls@uni-muenster.de (I.M.); alexander.hepp@uni-muenster.de (A.H.)
2 CeNTech, CiMIC, SoN, Universität Münster, Heisenbergstraße 11, 48149 Münster, Germany
3 Institute for Solid State Theory and Center for Multiscale Theory and Computation, Universität Münster,
Wilhelm-Klemm-Straße 10, 48149 Münster, Germany
4 European Institute for Molecular Imaging, Universität Münster, Röntgenstraße 16, 48149 Münster, Germany;
faustan@uni-muenster.de (A.F.)
5 Department of Nuclear Medicine, University Hospital Münster, Albert-Schweitzer-Campus 1,
48149 Münster, Germany
* Correspondence: ca.s@uni-muenster.de

Table of contents

Section S1: NMR spectra of **OMe**, **NMe$_2$**, **Zn-OMeNc**, **Zn-NMe$_2$Nc**, **Zn-NMe$_3$Nc** **03**

Section S2: Mass spectra of **OMe**, **NMe$_2$**, **Zn-OMeNc**, **Zn-NMe$_2$Nc**, **Zn-NMe$_3$Nc** **16**

Section S3: Photophysical characterization of **OMe**, **NMe$_2$**, **Zn-OMeNc**, **Zn-NMe$_2$Nc**, **Zn-NMe$_3$Nc** **18**

Section S4: DFT calculations **30**

Section S5: ZnNMe$_2$Nc loaded onto polystyrene microparticles (PSMPs) **33**

Section S1: NMR spectra of OMe, NMe_2, Zn-OMeNc, Zn-NMe_2Nc, Zn-NMe_3Nc

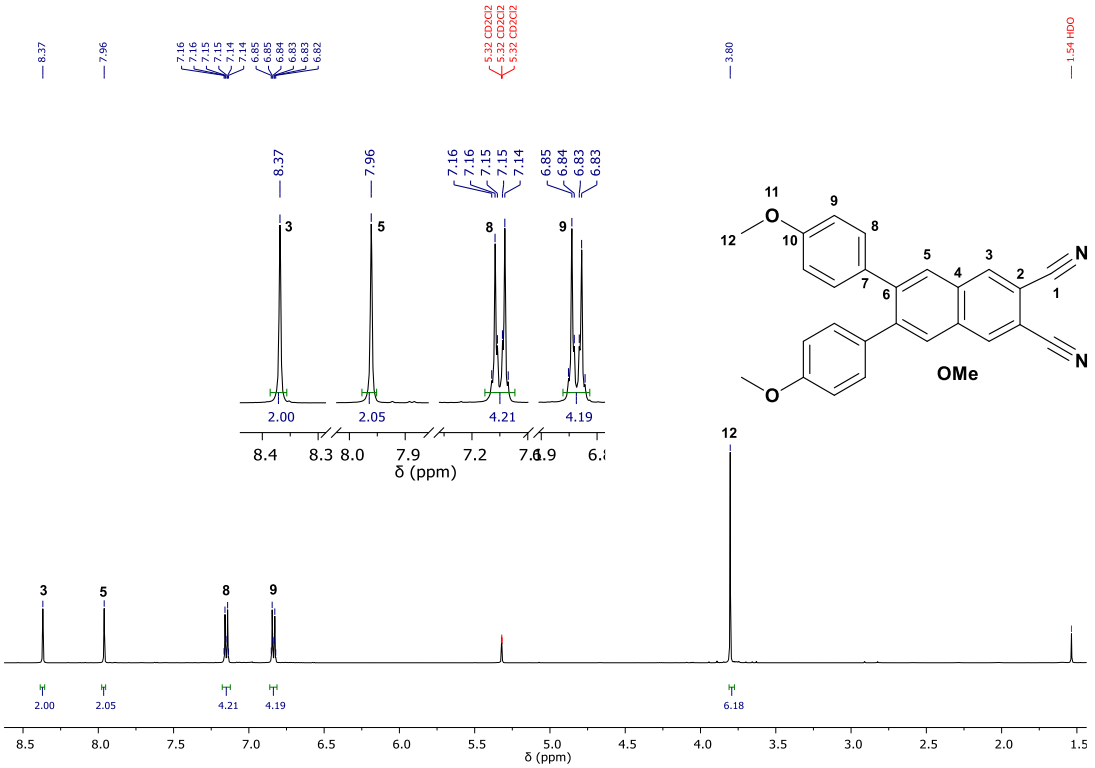


Fig. S1 ^{1}H-NMR spectrum (500 MHz, DCM-d_2) of **OMe**.

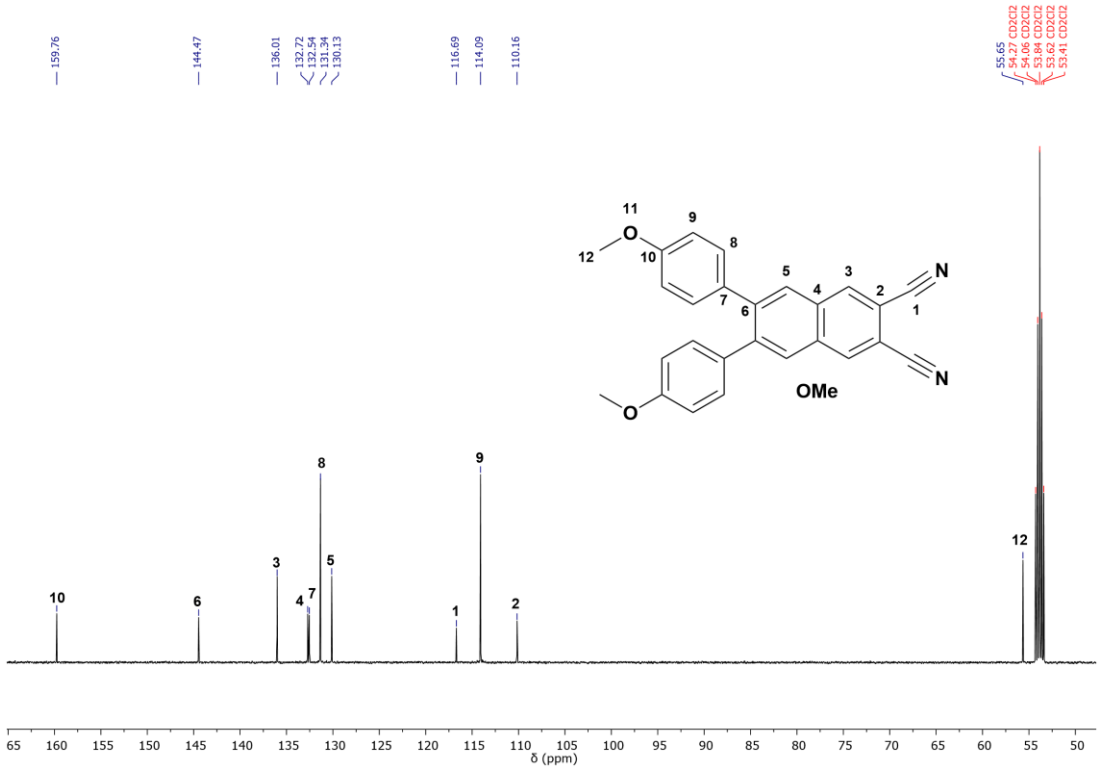


Fig. S2 ^{13}C-{^{1}H}-NMR spectrum (126 MHz, DCM-d_2) of **OMe**).

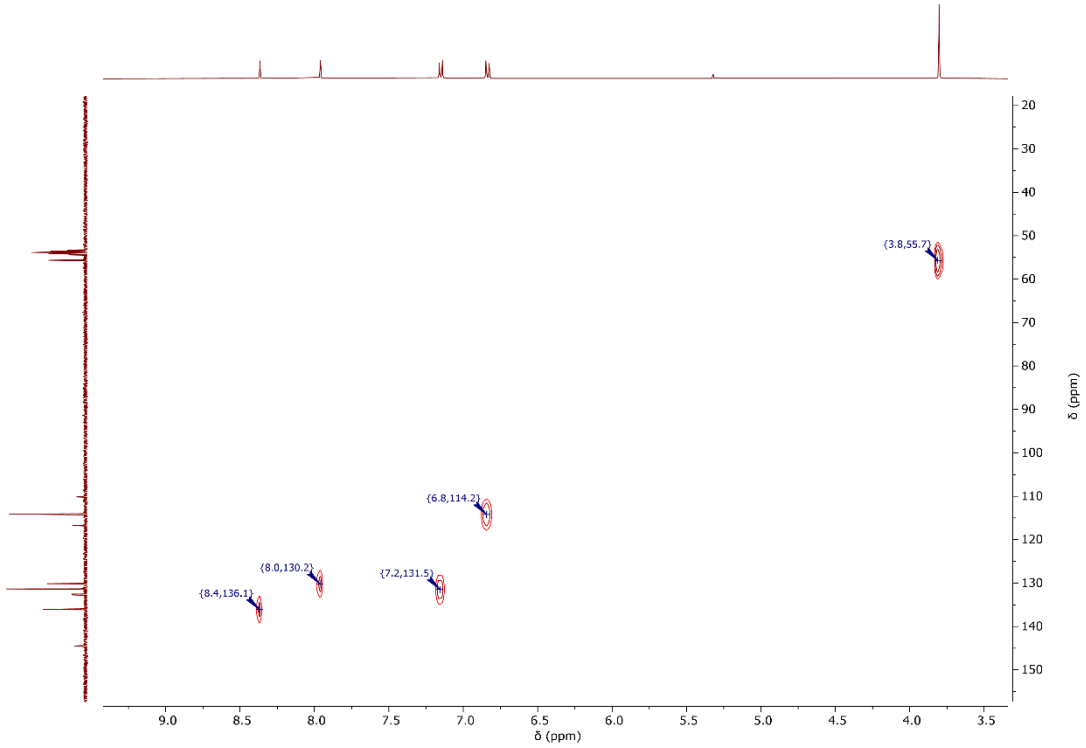


Fig. S3 $^{1}H/^{13}C$-gHSQC-NMR spectrum (400 MHz/101 MHz, DCM-d_2) of **OMe**.

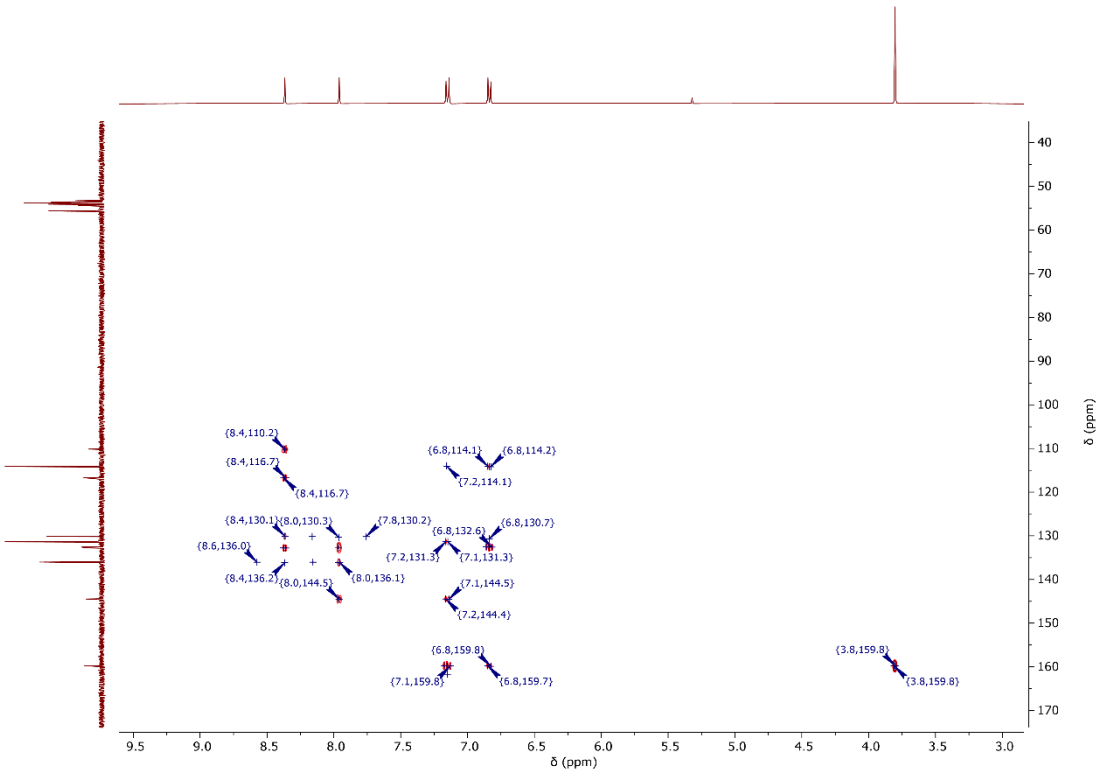


Fig. S4 $^{1}H/^{13}C$-gHMBC-NMR spectrum (400 MHz/101 MHz, DCM-d_2) of **OMe**.

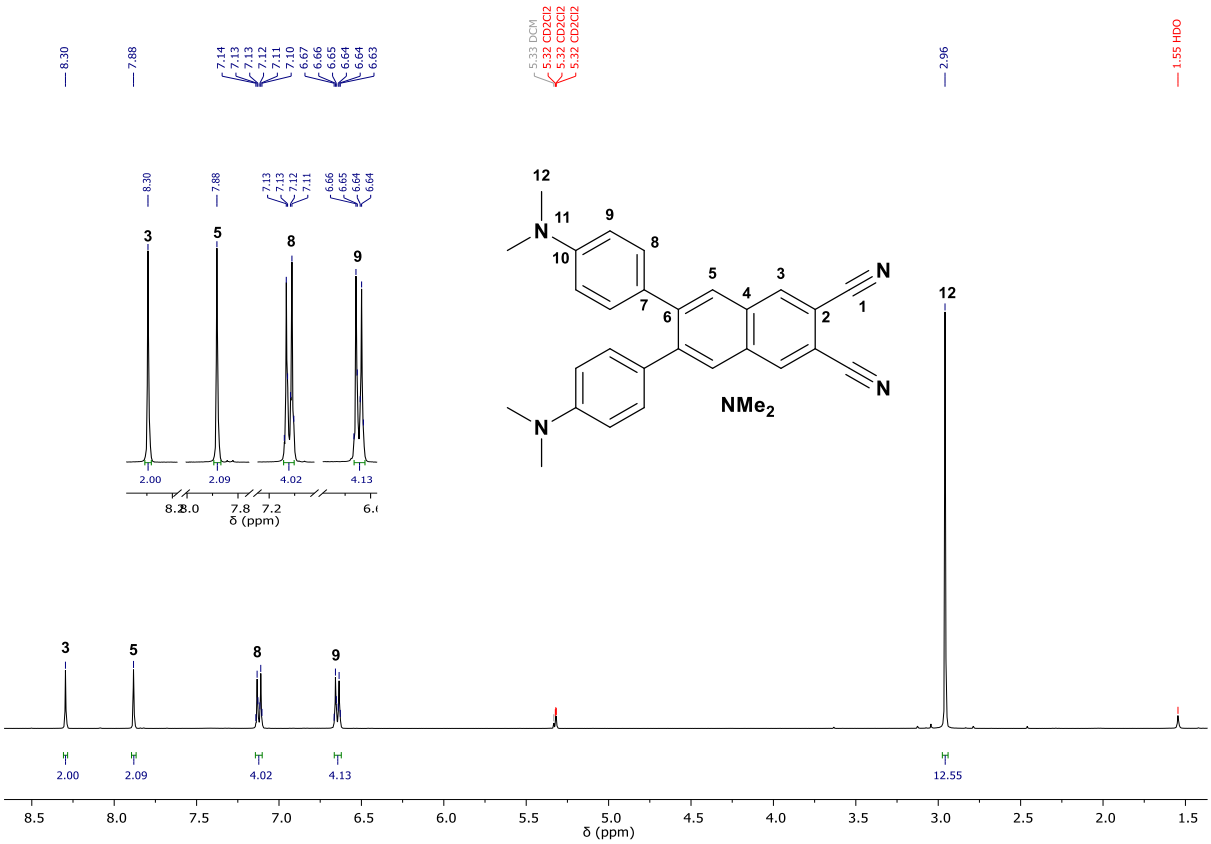


Fig. S5 ^{1}H-NMR spectrum (500 MHz, DCM-d_2) of **NMe_2**.

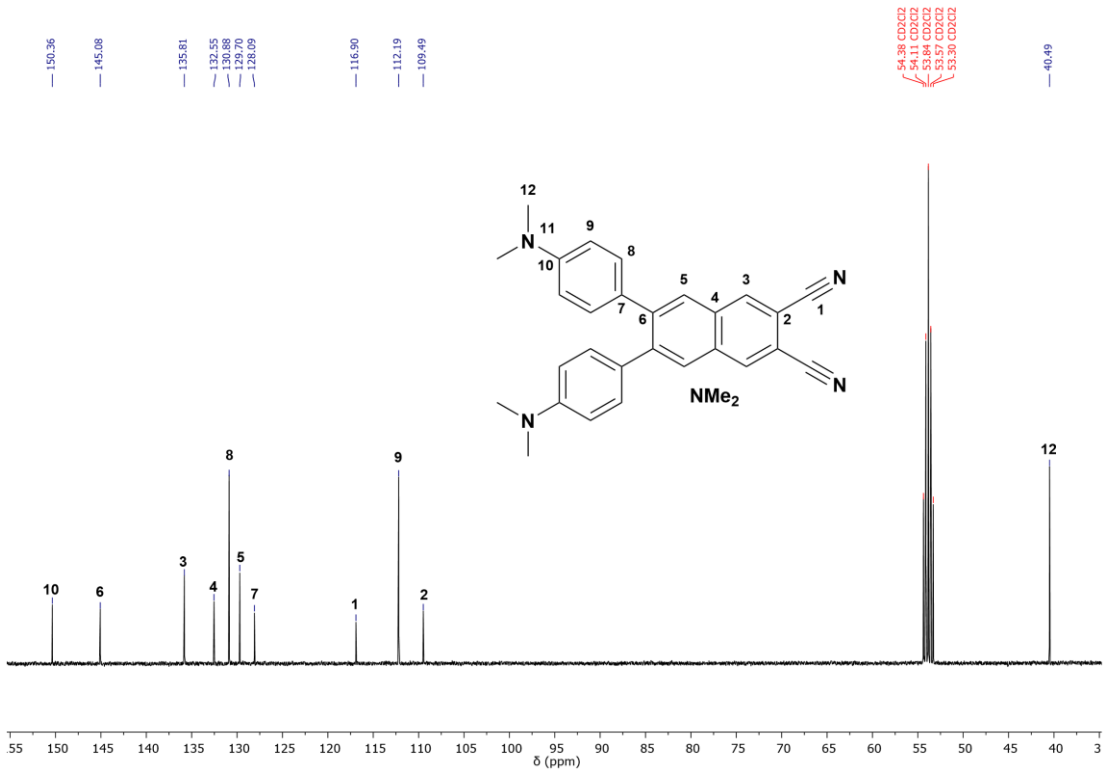


Fig. S6 ^{13}C-{^{1}H}-NMR spectrum (126 MHz, DCM-d_2) of **NMe_2**.

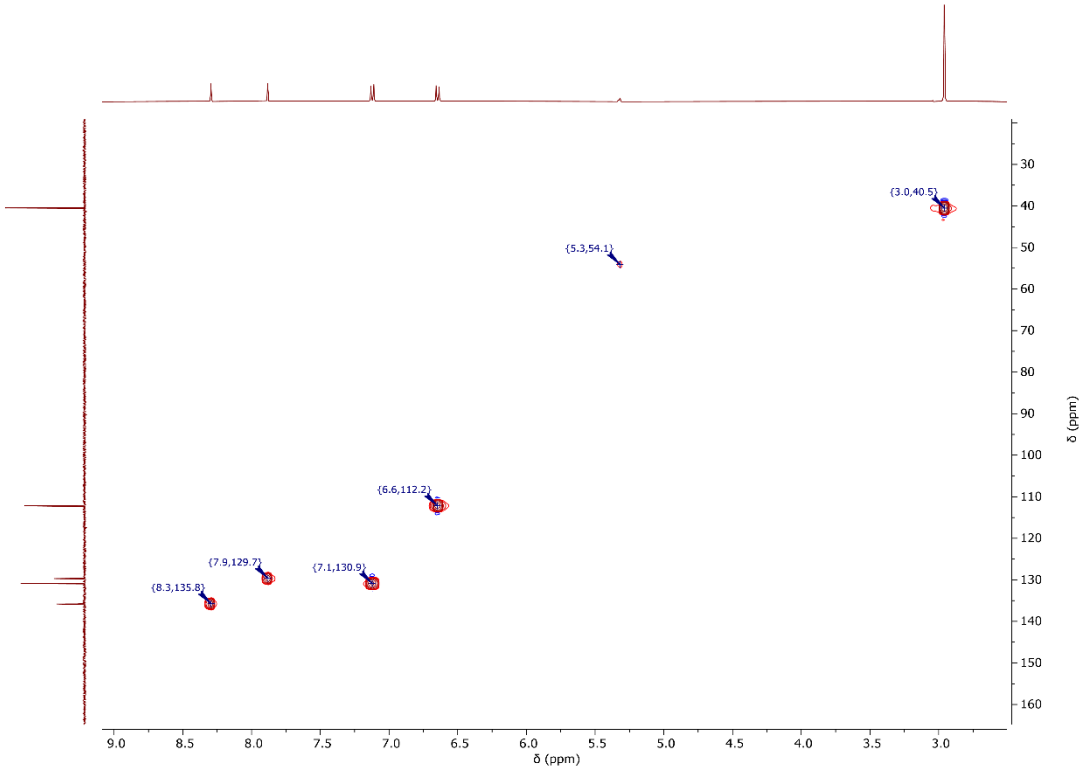


Fig. S7 $^{1}H/^{13}C$-gHSQC-NMR spectrum (400 MHz/101 MHz, DCM-d_2) **NMe$_2$**.

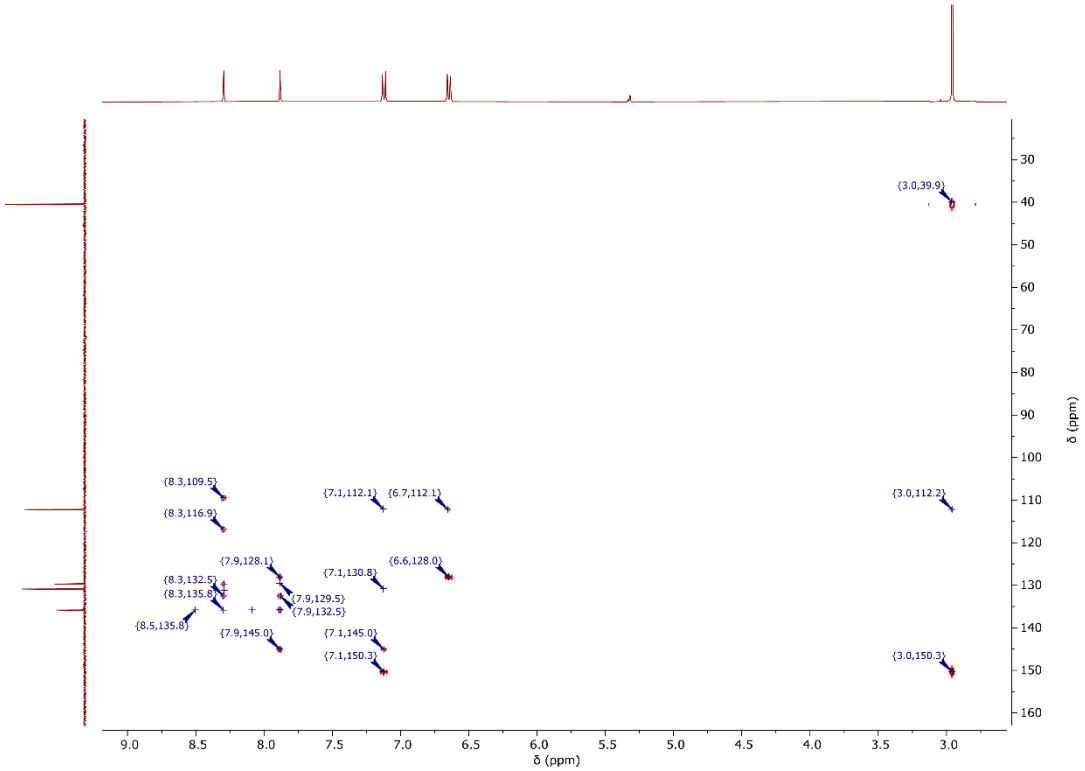


Fig. S8 $^{1}H/^{13}C$-gHMBC-NMR spectrum (400 MHz/101 MHz, DCM-d_2) of **NMe$_2$**.

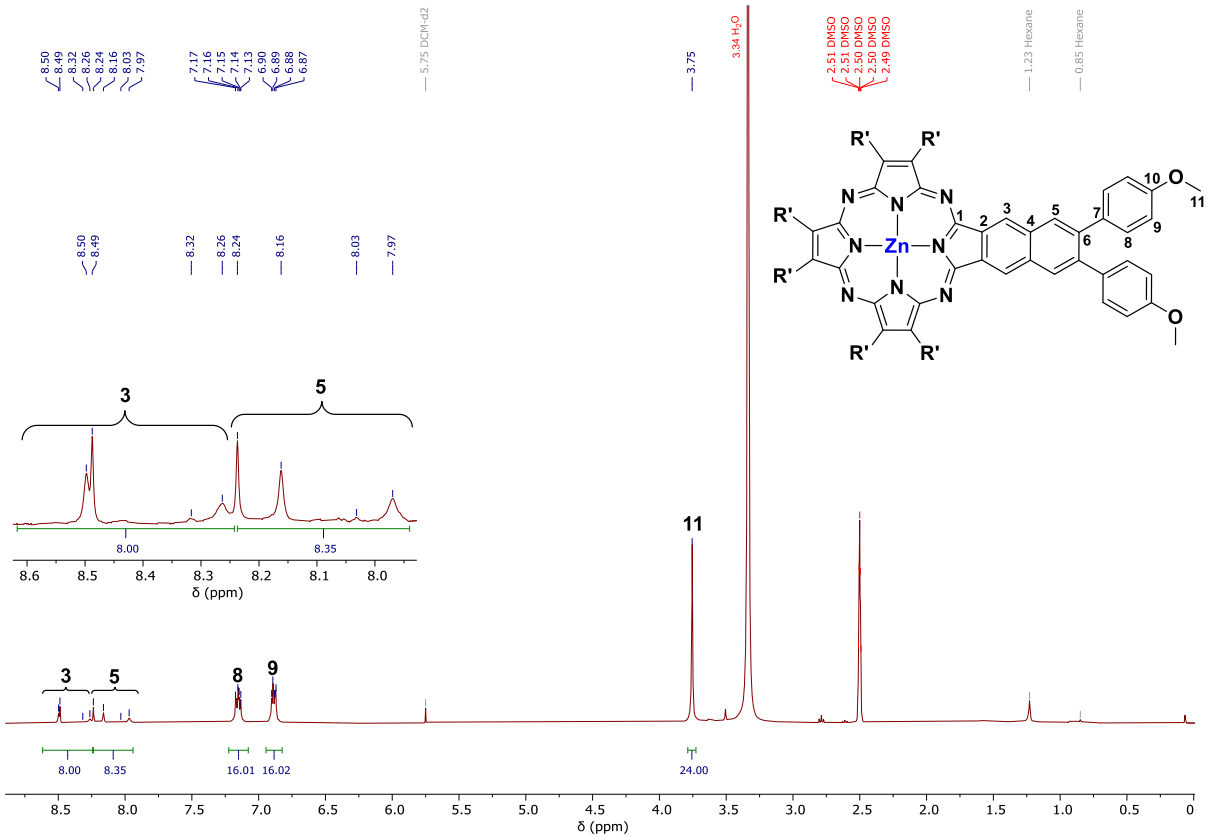


Fig. S9 ^{1}H-NMR spectrum (400 MHz, DMSO-d_6) of **Zn-OMeNc**.

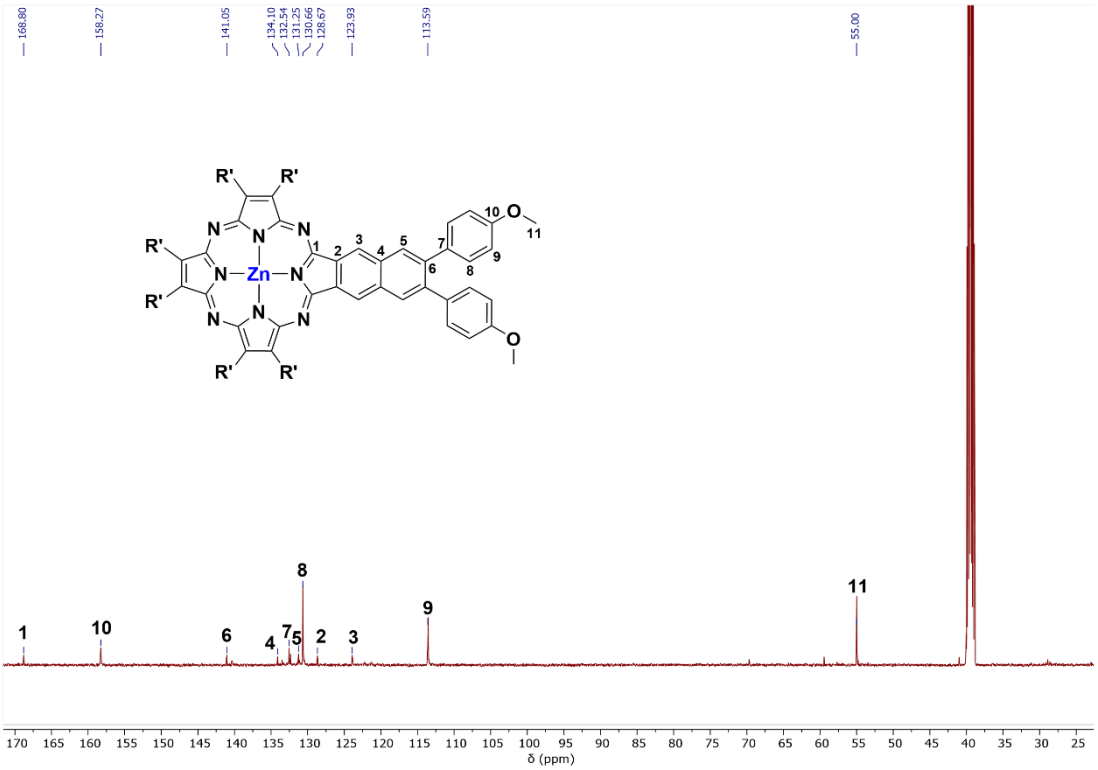


Fig. S10 ^{13}C-{^{1}H}-NMR spectrum (126 MHz, DMSO-d_6) of **Zn-OMeNc.**

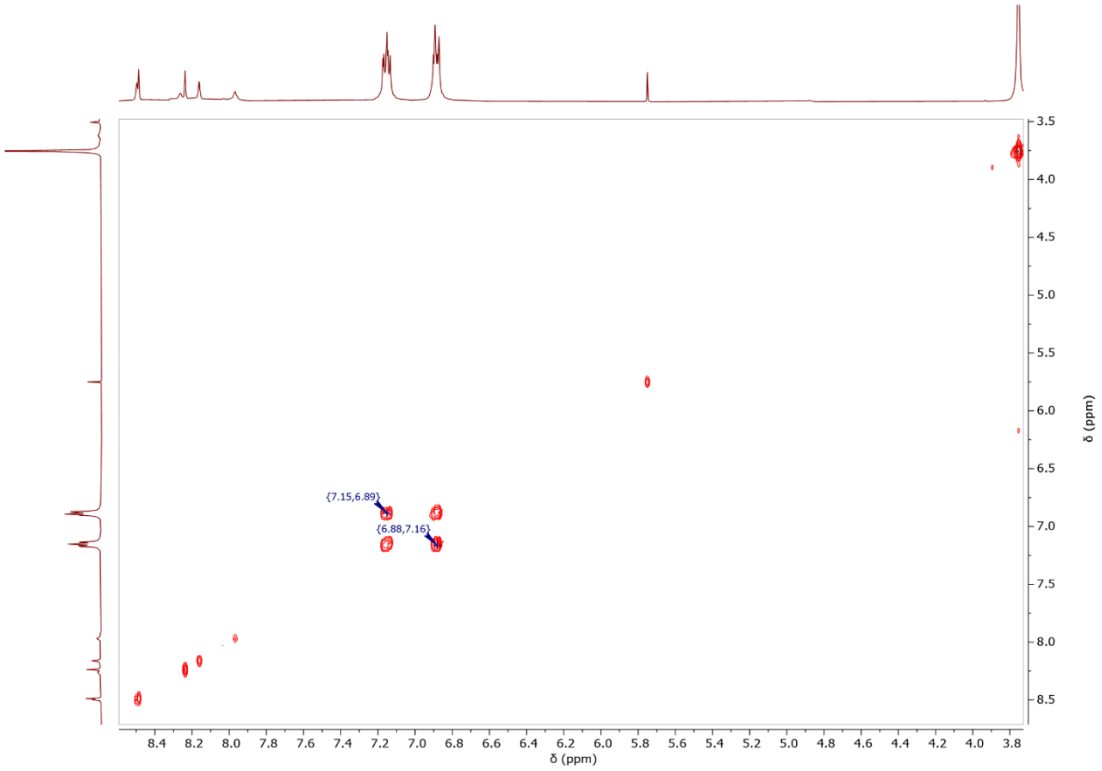


Fig. S11 ^{1}H-^{1}H-COSY-NMR spectrum (500 MHz, DMSO-d_6) of **Zn-OMeNc**.

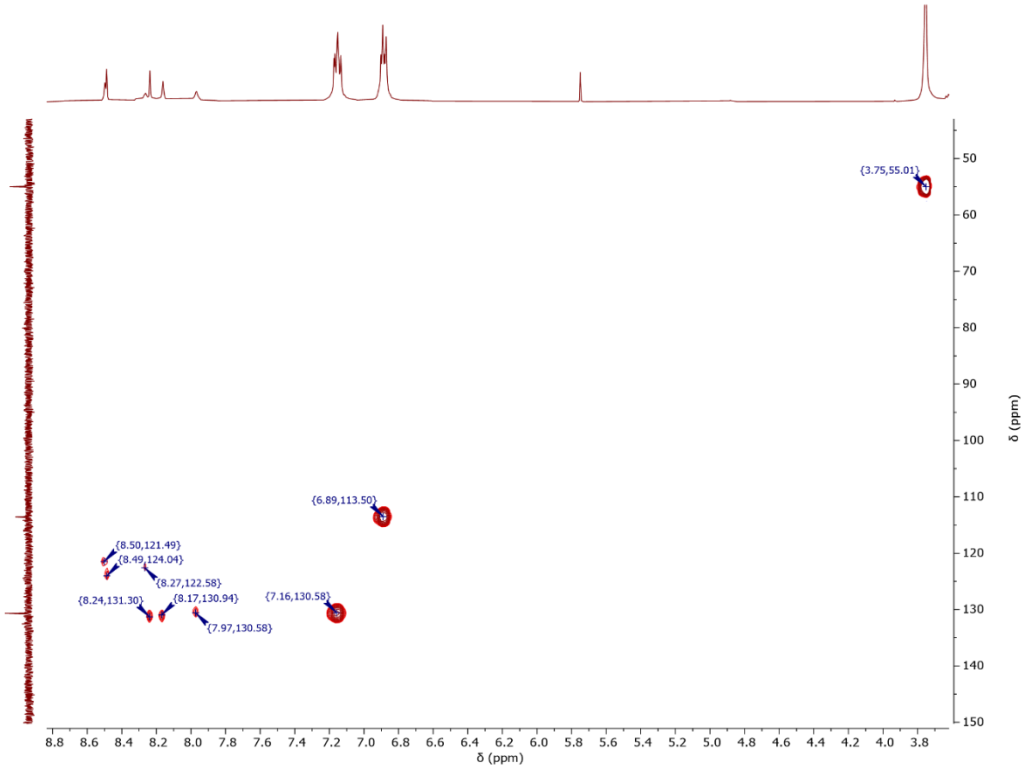


Fig. S12 ^{1}H/^{13}C-gHSQC-NMR spectrum (400 MHz/101 MHz, DMSO-d_6) of **Zn-OMeNc**.

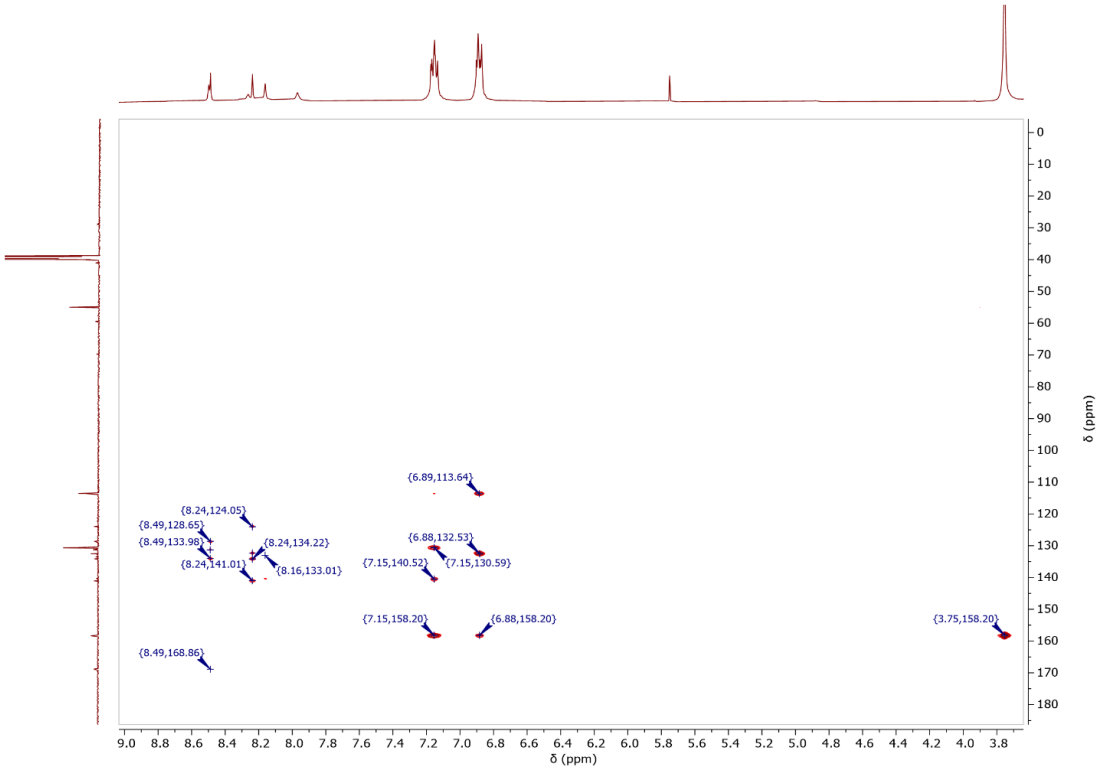


Fig. S13 $^{1}H/^{13}C$-gHMBC-NMR spectrum (400 MHz/101 MHz, DMSO-d_6) of **Zn-OMeNc**.

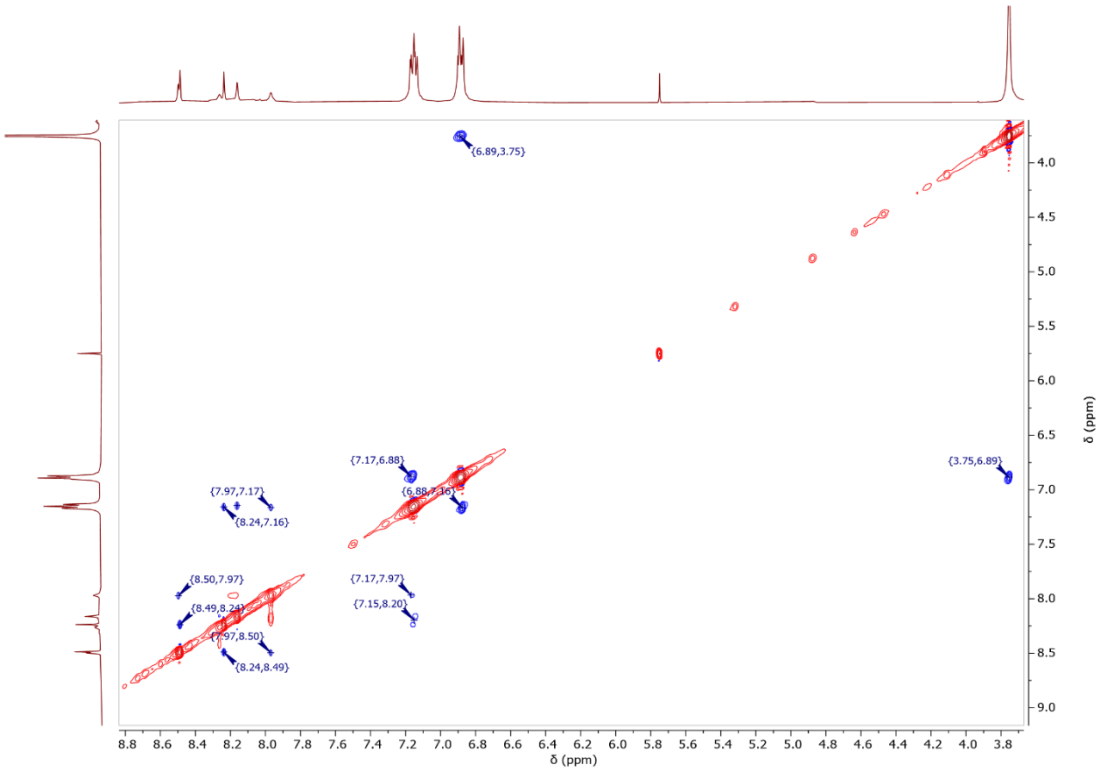


Fig. S14 ^{1}H-^{1}H-ROESY-NMR spectrum (500 MHz, DMSO-d_6) of **Zn-OMeNc**.

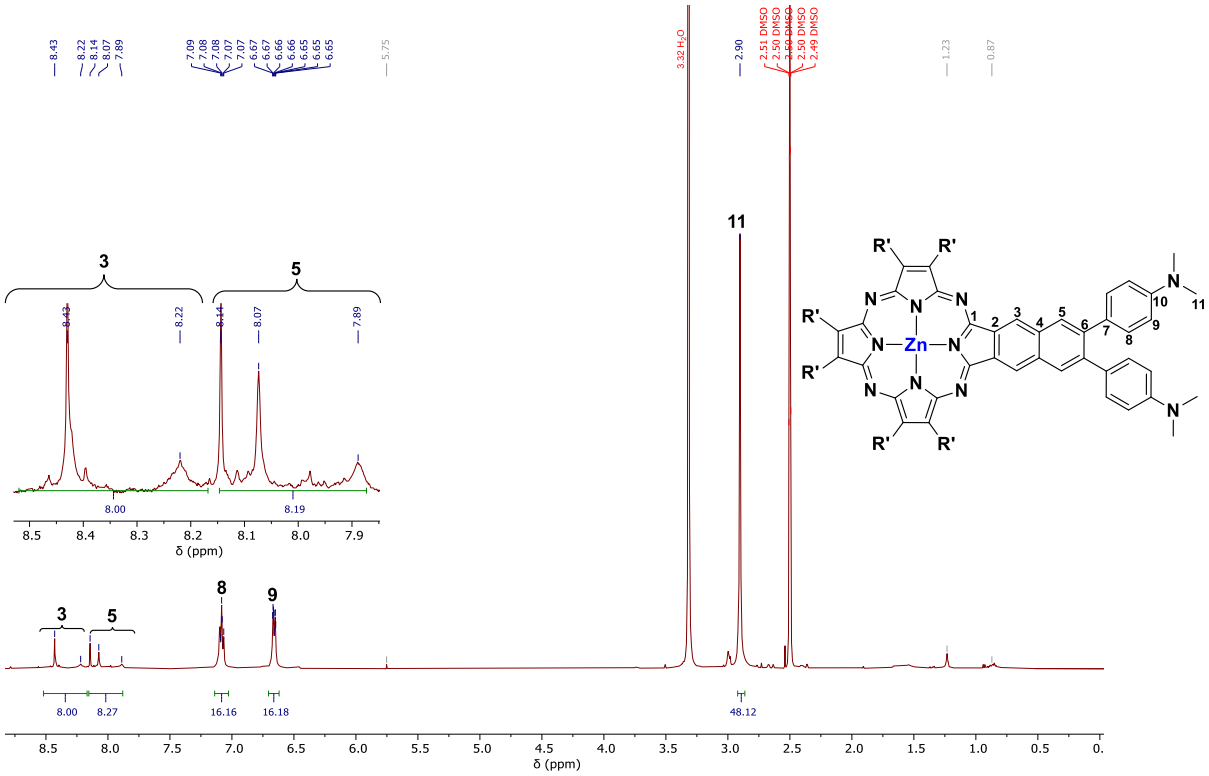


Fig. S15 ^{1}H-NMR spectrum (400 MHz, DMSO-d_6) of **Zn-NMe$_2$Nc**.

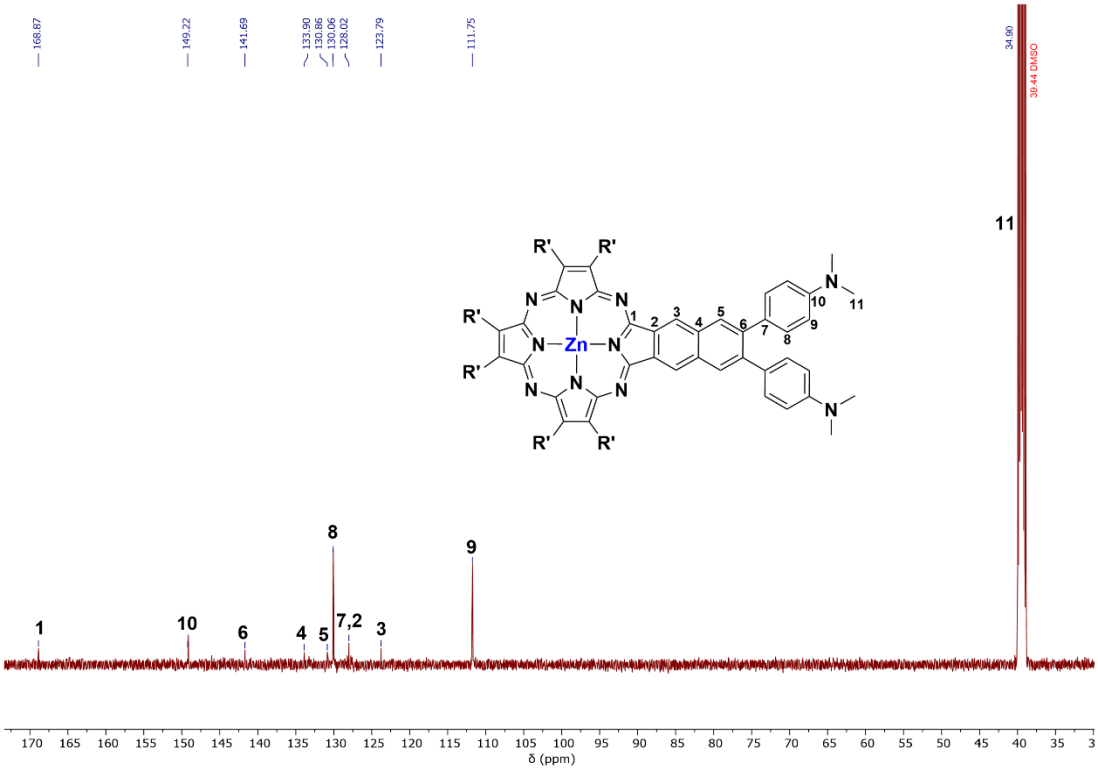


Fig. S16 ^{13}C-{^{1}H}-NMR spectrum (100 MHz, DMSO-d_6) of **Zn-NMe$_2$Nc**.

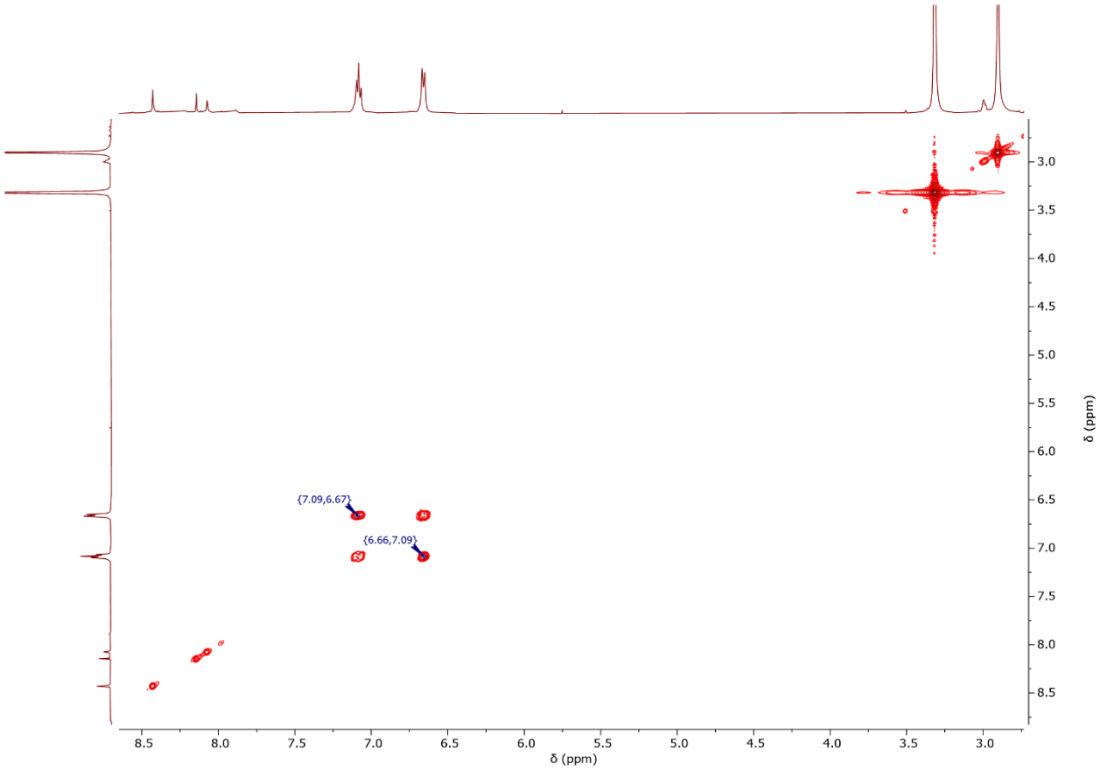


Fig. S17 ^{1}H-^{1}H-COSY-NMR spectrum (400 MHz, DMSO-d_6) of **Zn-NMe$_2$Nc**.

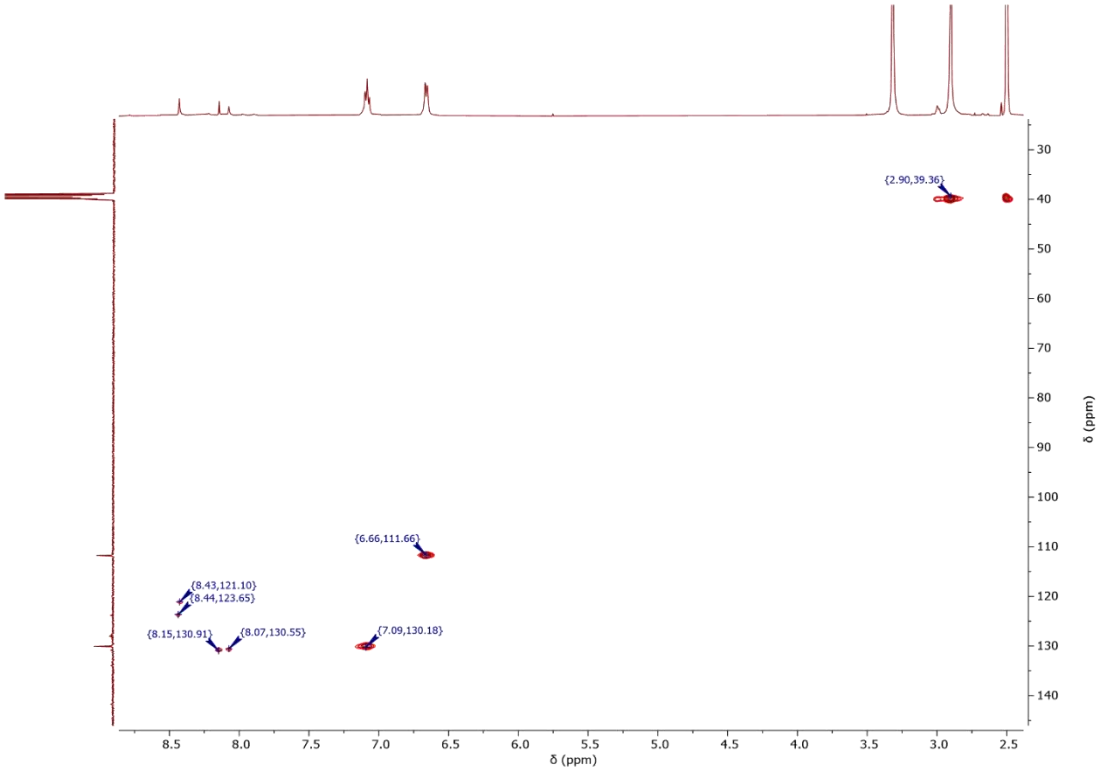


Fig. S18 ^{1}H/^{13}C-gHSQC-NMR spectrum (400 MHz, DMSO-d_6) of **Zn-NMe$_2$Nc**.

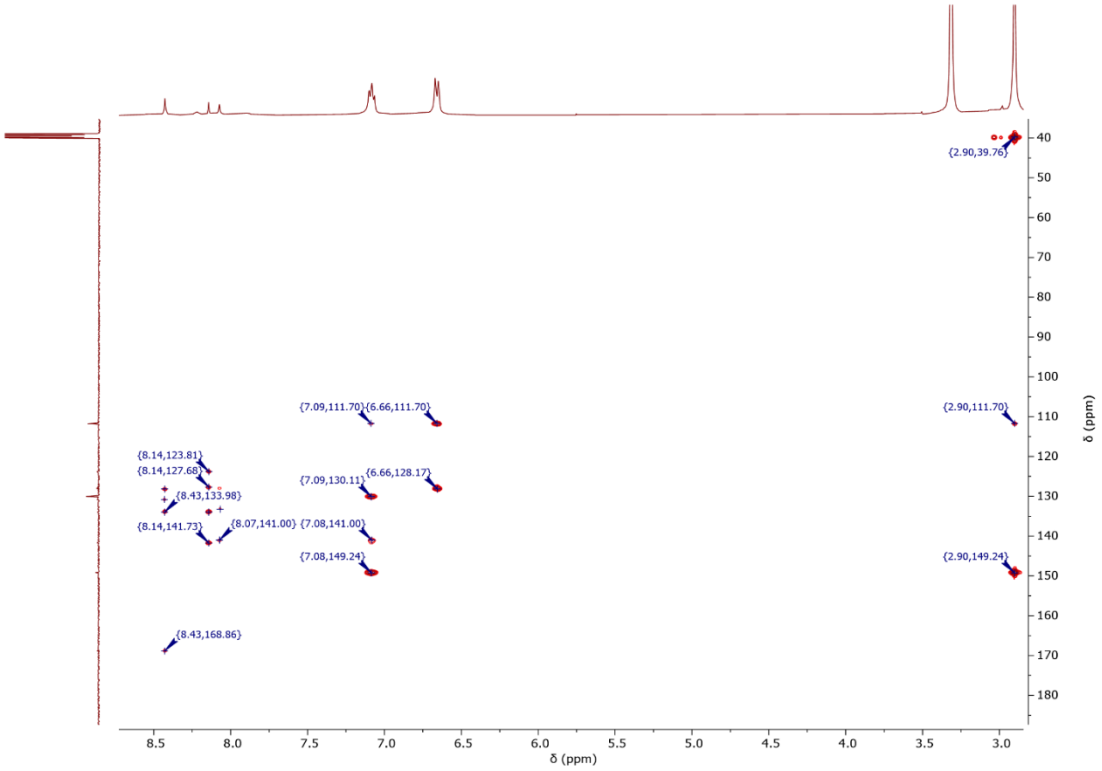


Fig. S19 $^{1}H/^{13}C$-gHMBC-NMR spectrum (400 MHz, DMSO-d_6) of **Zn-NMe$_2$Nc**.

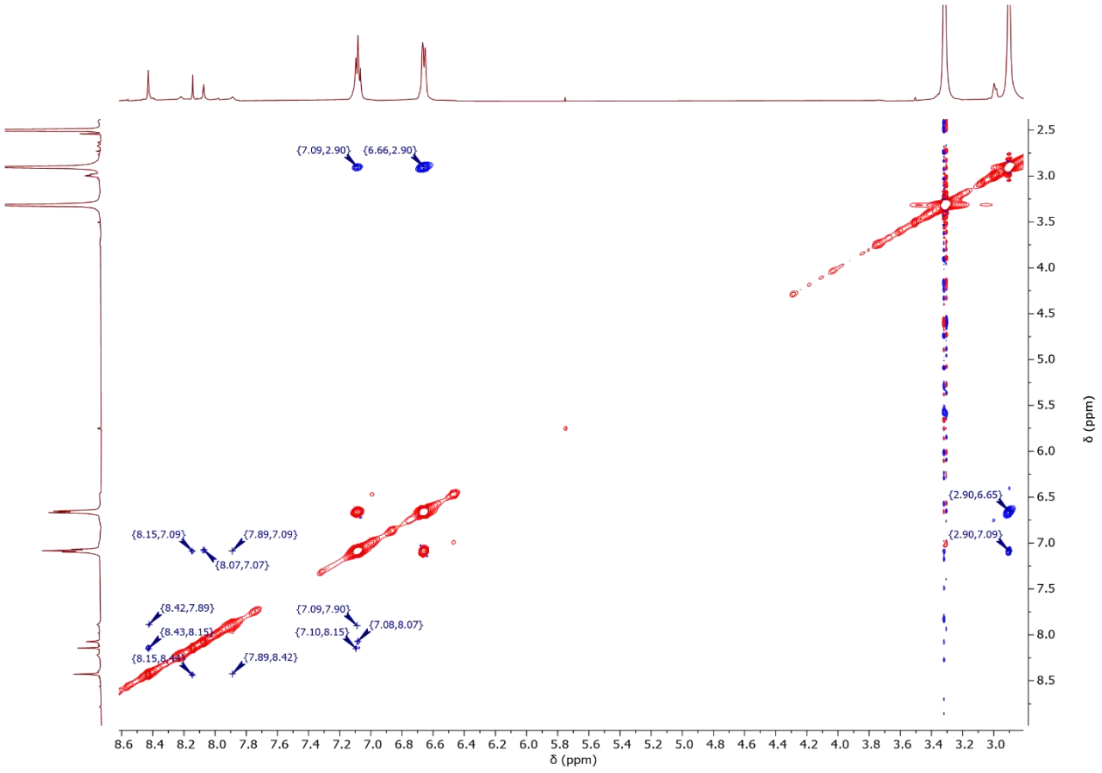


Fig. S20 ^{1}H-^{1}H-ROESY-NMR spectrum (400 MHz, DMSO-d_6) of **Zn-NMe$_2$Nc**.

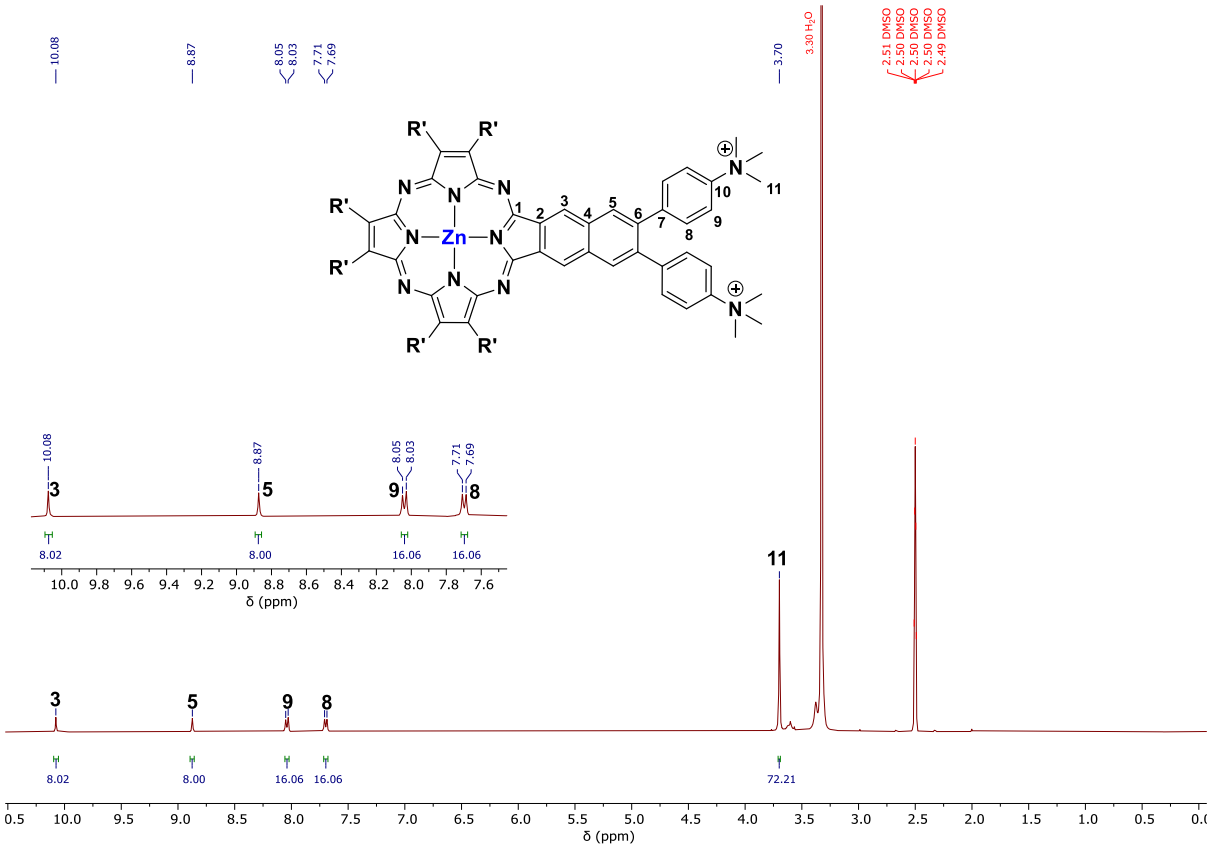


Fig. S21 ^{1}H-NMR spectrum (400 MHz, DMSO-*d*$_6$) of **Zn-NMe$_3$Nc**.

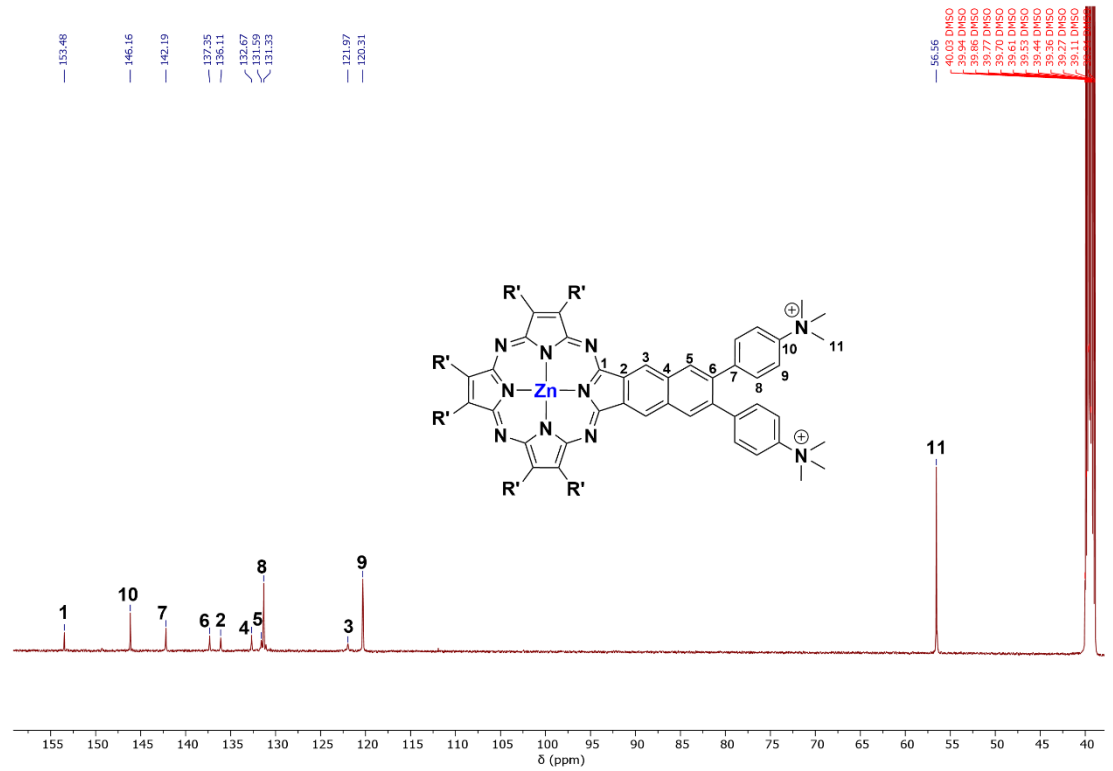


Fig. S22 ^{13}C-{^{1}H}-NMR spectrum (126 MHz, DMSO-*d*$_6$) of **Zn-NMe$_3$Nc**.

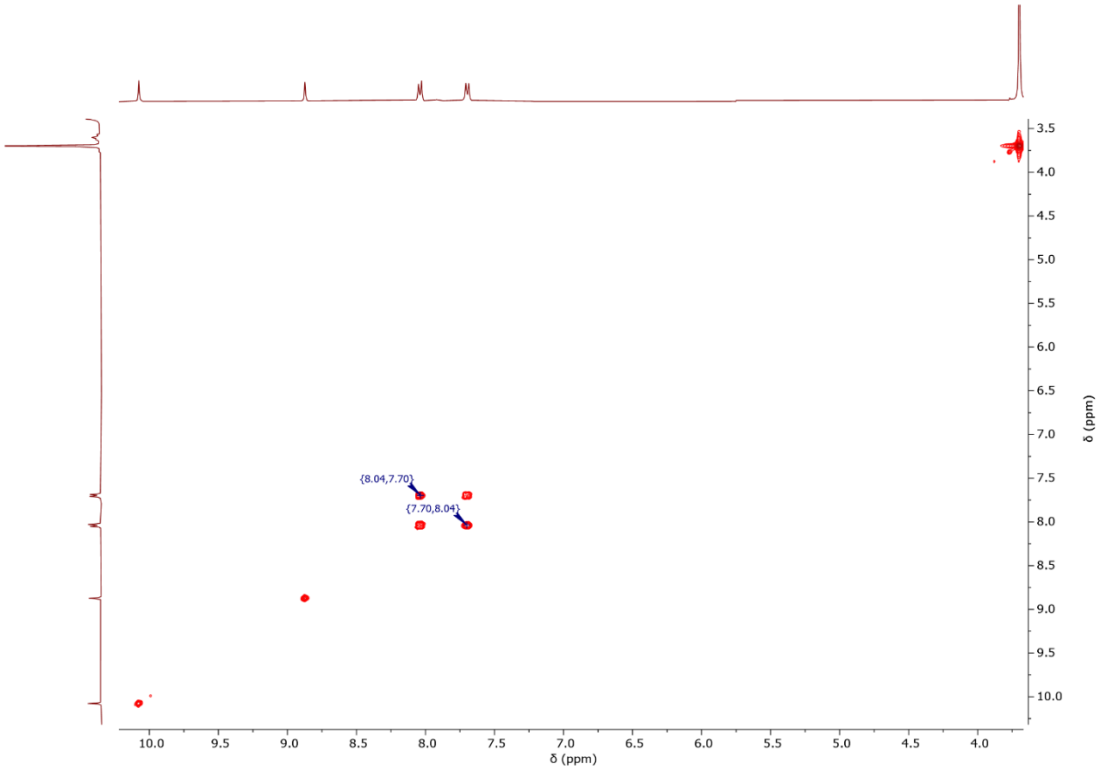


Fig. S23 ^{1}H-^{1}H-COSY-NMR spectrum (400 MHz, DMSO-*d*$_6$) of **Zn-NMe$_3$Nc**.

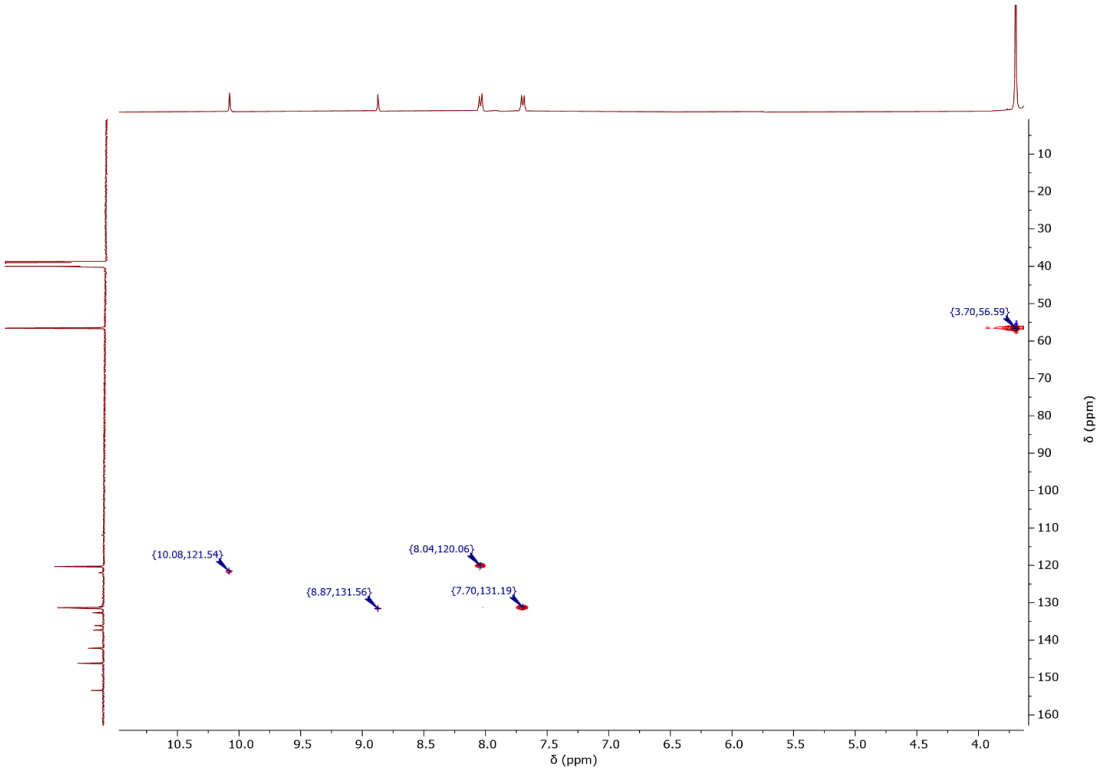


Fig. S24 ^{1}H/^{13}C-gHSQC-NMR spectrum (400 MHz/101 MHz, DMSO-*d*$_6$) of **Zn-NMe$_3$Nc**.

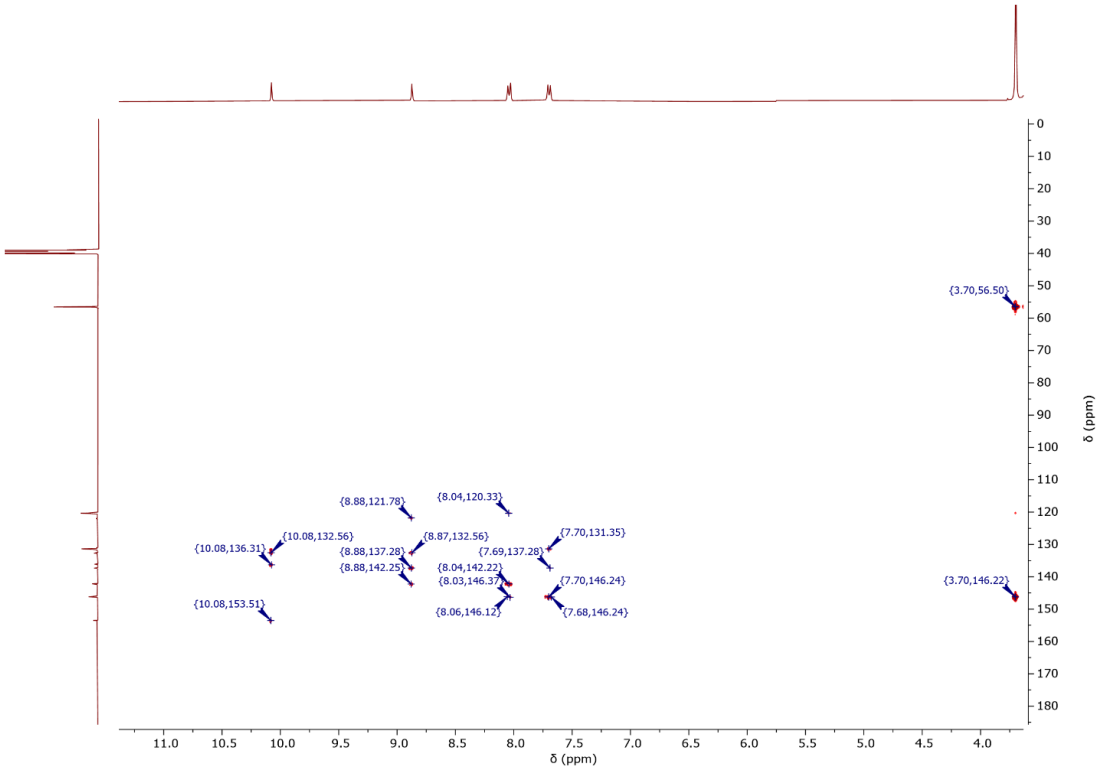


Fig. S25 $^{1}H/^{13}C$-gHMBC-NMR spectrum (400 MHz/101 MHz, DMSO-d_6) of **Zn-NMe$_3$Nc**.

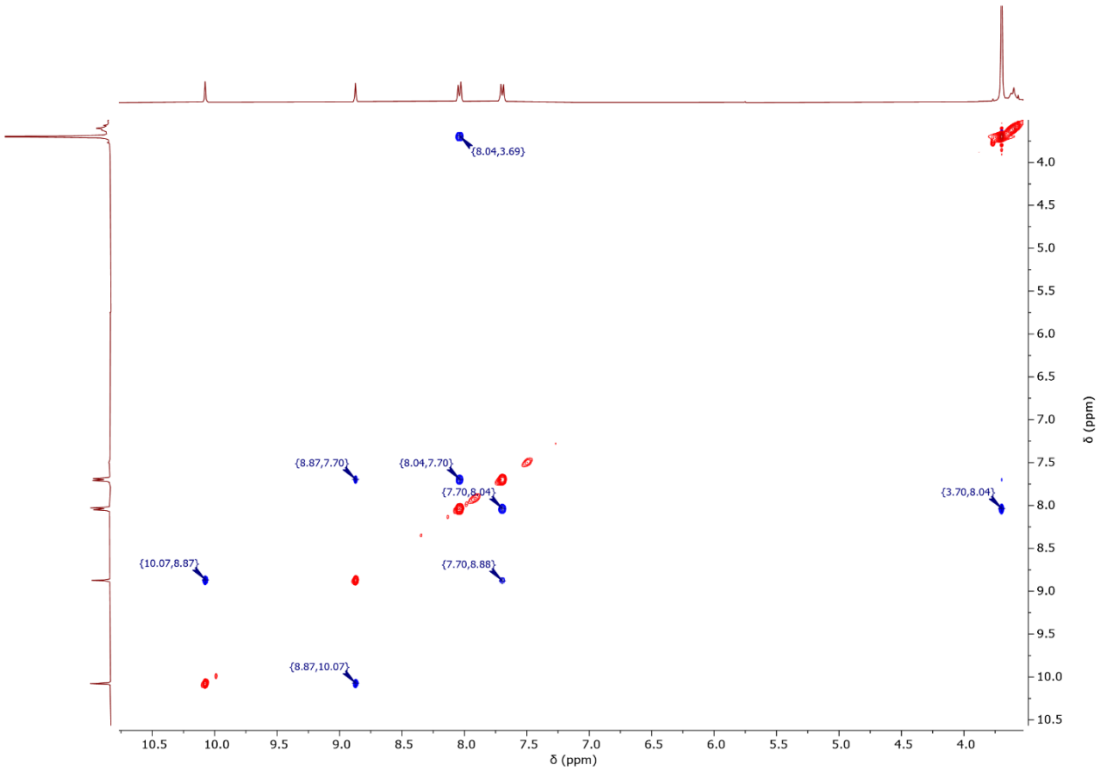


Fig. S26 ^{1}H-^{1}H-ROESY-NMR spectrum (400 MHz, DMSO-d_6) of **Zn-NMe$_3$Nc**.

Section S2: Mass spectra of OMe, NMe_2, Zn-OMeNc, Zn-NMe_2Nc, Zn-NMe_3Nc

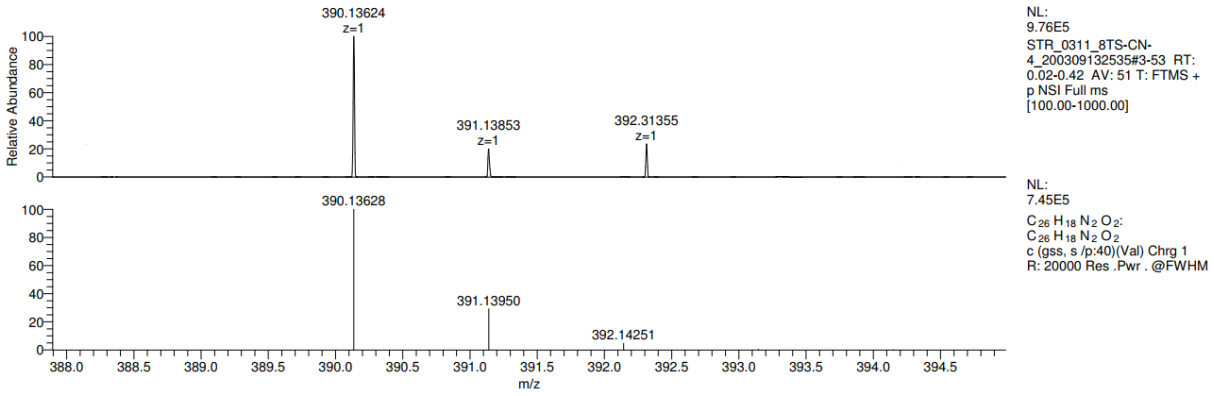


Fig. S27 EM-MS-ESI spectrum of **OMe**.

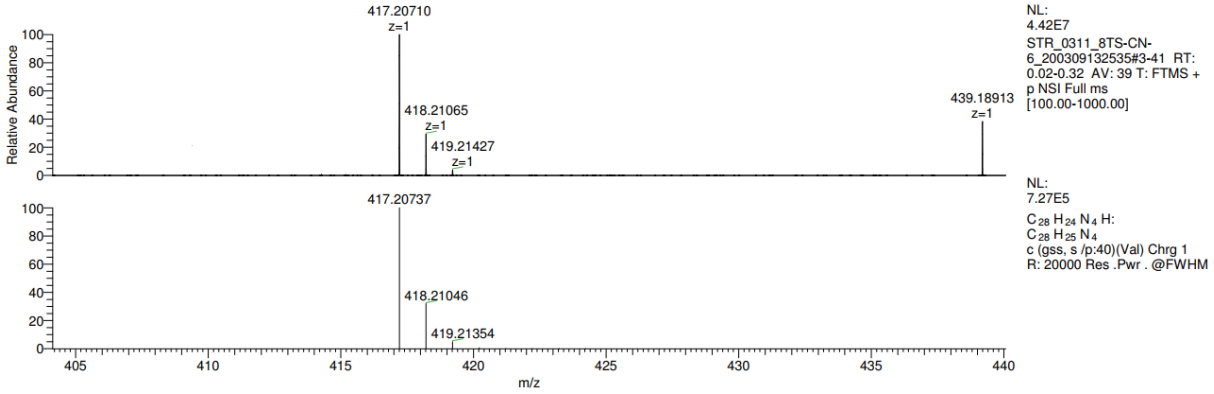


Fig. S28 EM-MS-ESI spectrum of **NMe_2**.

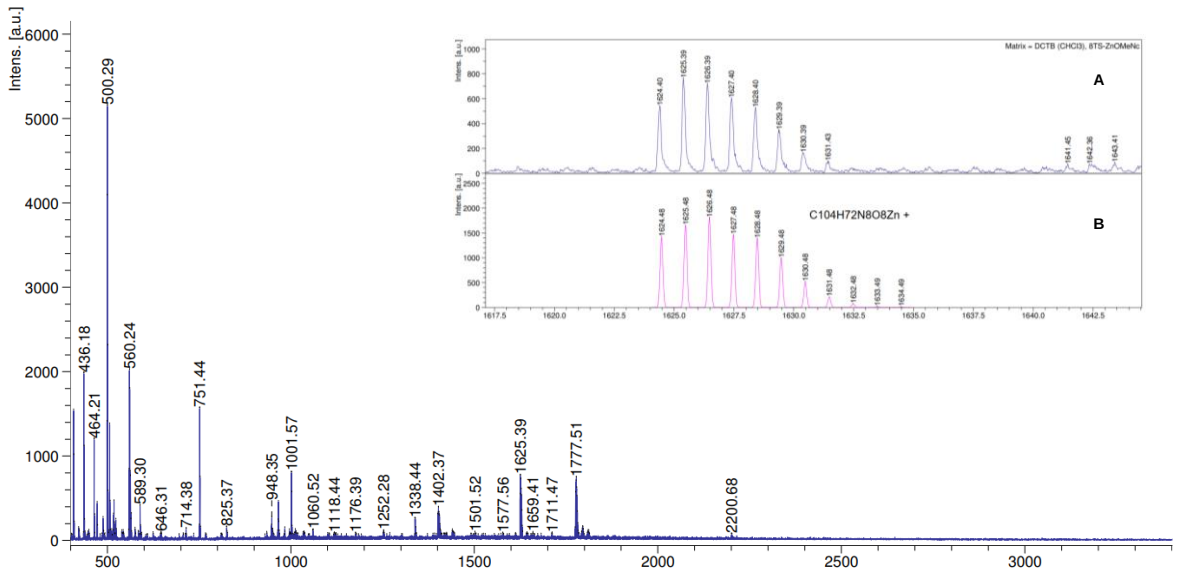


Fig. S29 MALDI-TOF mass spectrum of **Zn-OMeNc**, isotopic patterns for the molecular ion (inset A) and simulated MS patterns of the molecular ion (inset B).

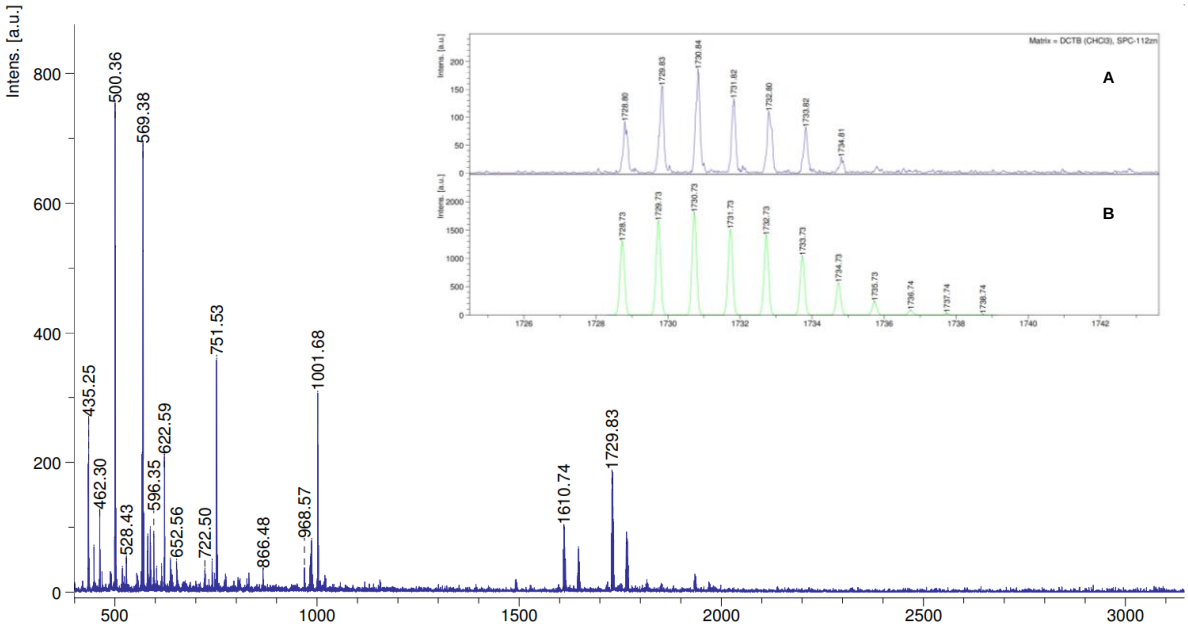


Fig. S30 MALDI-TOF mass spectrum of **Zn-NMe$_2$Nc**, isotopic patterns for the molecular ion (inset A) and simulated MS patterns of the molecular ion (inset B).

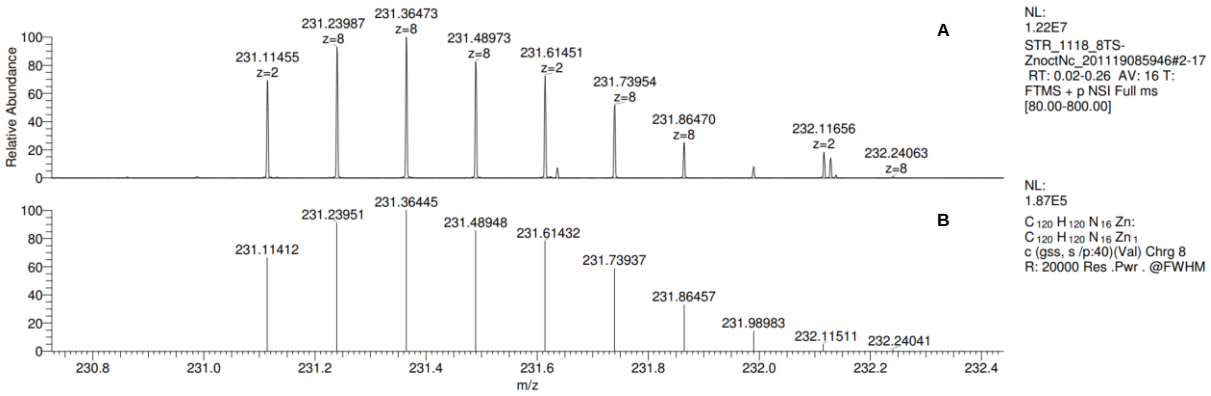


Fig. S31 EM-MS-ESI spectrum of **Zn-NMe$_3$Nc**, isotopic patterns for the molecular ion (inset A) and simulated MS patterns of the molecular ion (inset B).

Section S3: Photophysical characterization of Zn-OMeNc, Zn-NMe_2Nc, Zn-NMe_3Nc

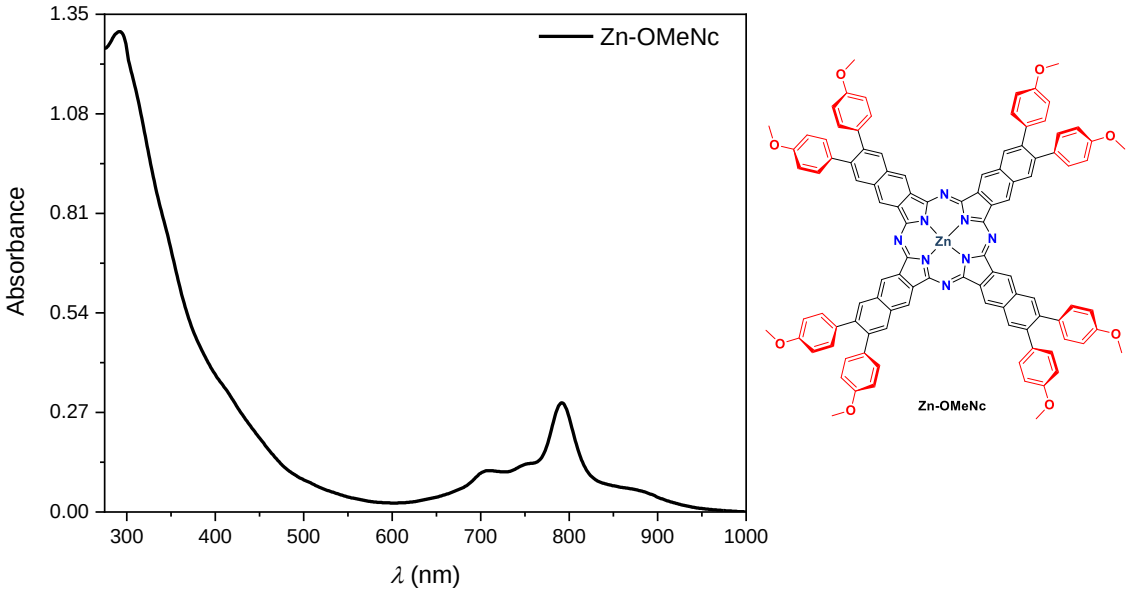


Fig. S32 UV-vis absorption spectrum of **Zn-OMeNc** in liquid DMSO at 298 K (λ_{max} = 794 nm).

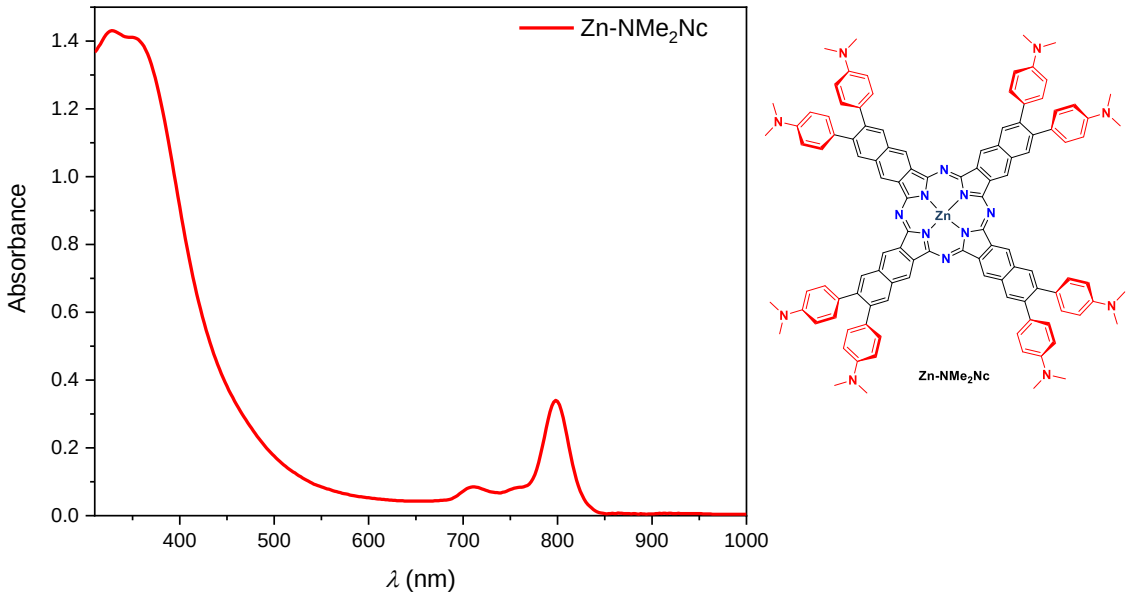


Fig. S33 UV-vis absorption spectrum of **Zn-NMe_2Nc** in liquid DMSO at 298 K (λ_{max} = 800 nm).

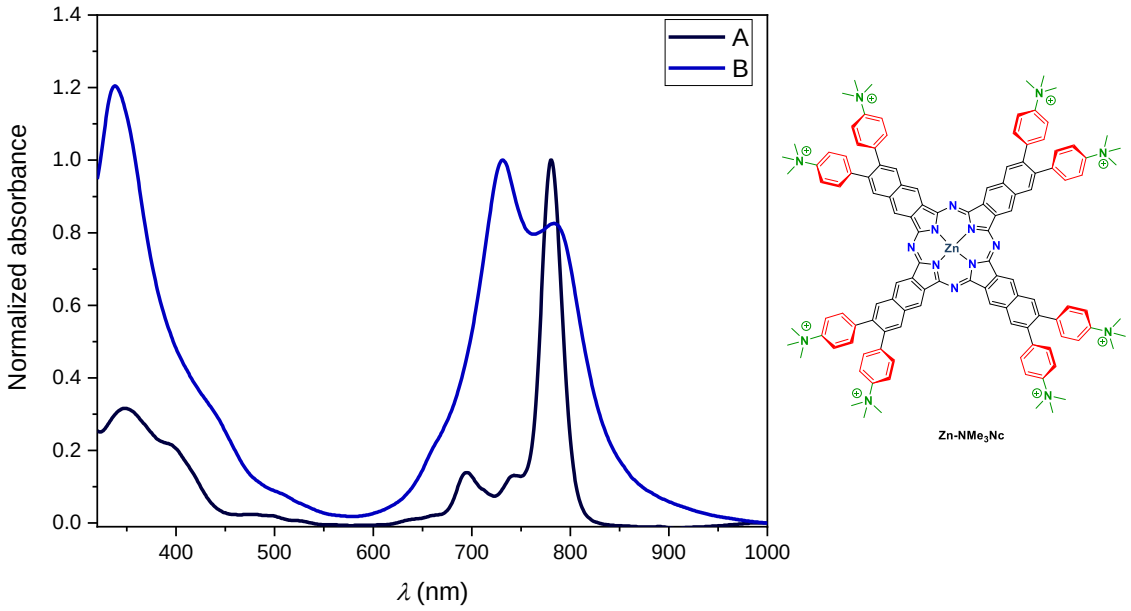


Fig. S34 UV-vis absorption spectra of **Zn-NMe$_3$Nc** in liquid DMSO (A) (λ_{max} = 781 nm) and water (B) (λ_{max} = 732, 784 nm) at 298 K.

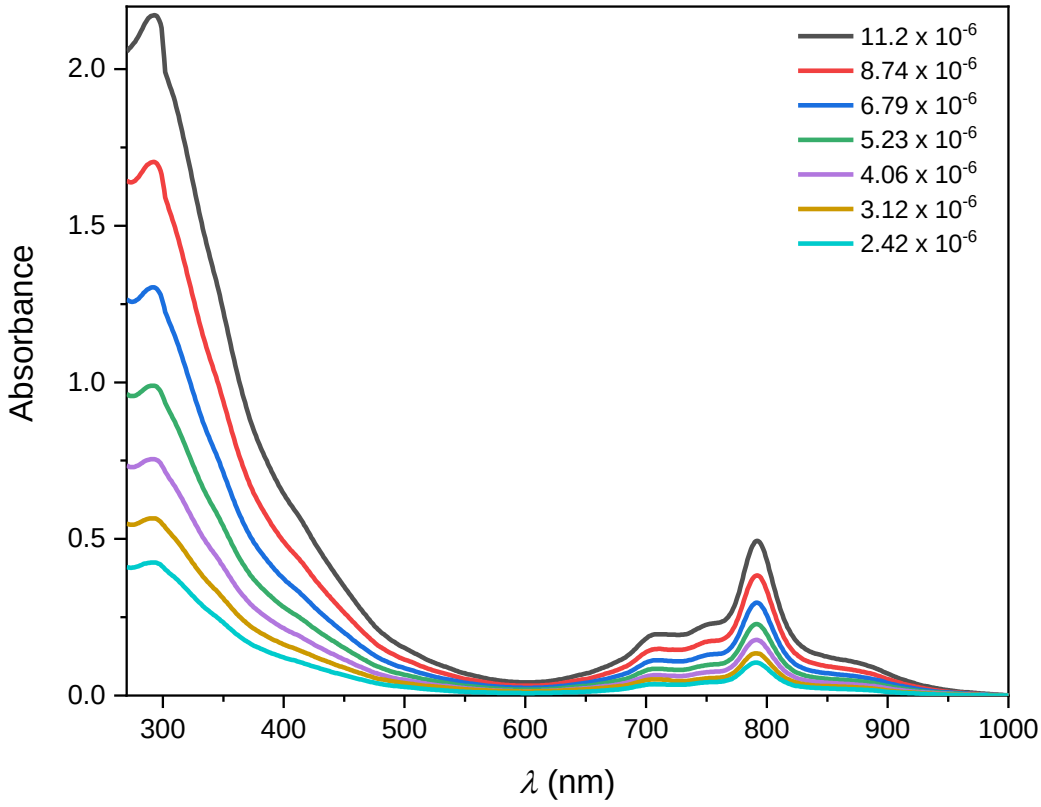


Fig. S35 UV-vis absorption spectra of **Zn-OMeNc** in liquid DMSO at different concentrations.

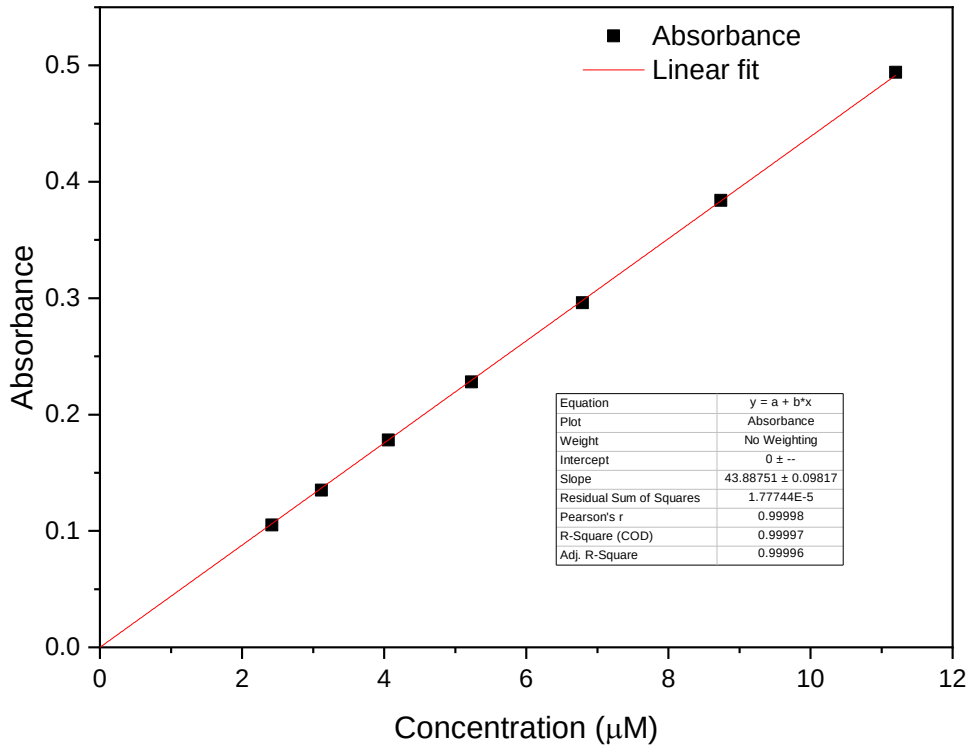


Fig. S36 Lambert-Beer law verified for **Zn-OMeNc** in liquid DMSO at 298 K (λ_{max} = 794 nm).

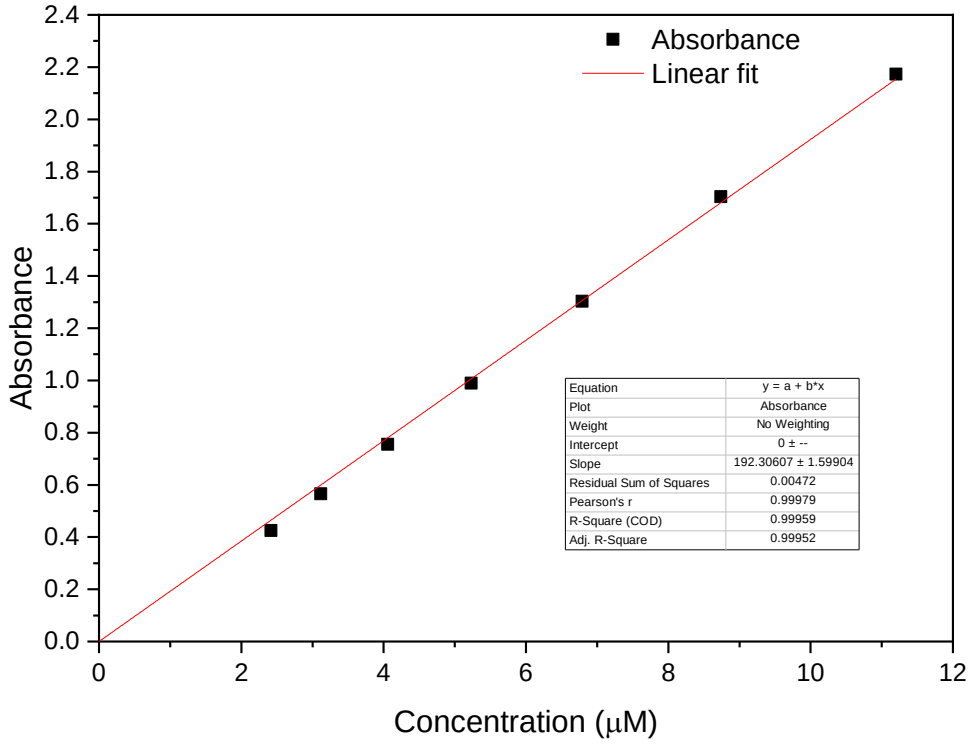


Fig. S37 Lambert-Beer law verified for **Zn-OMeNc** in liquid DMSO at 298 K (λ_{max} = 293 nm).

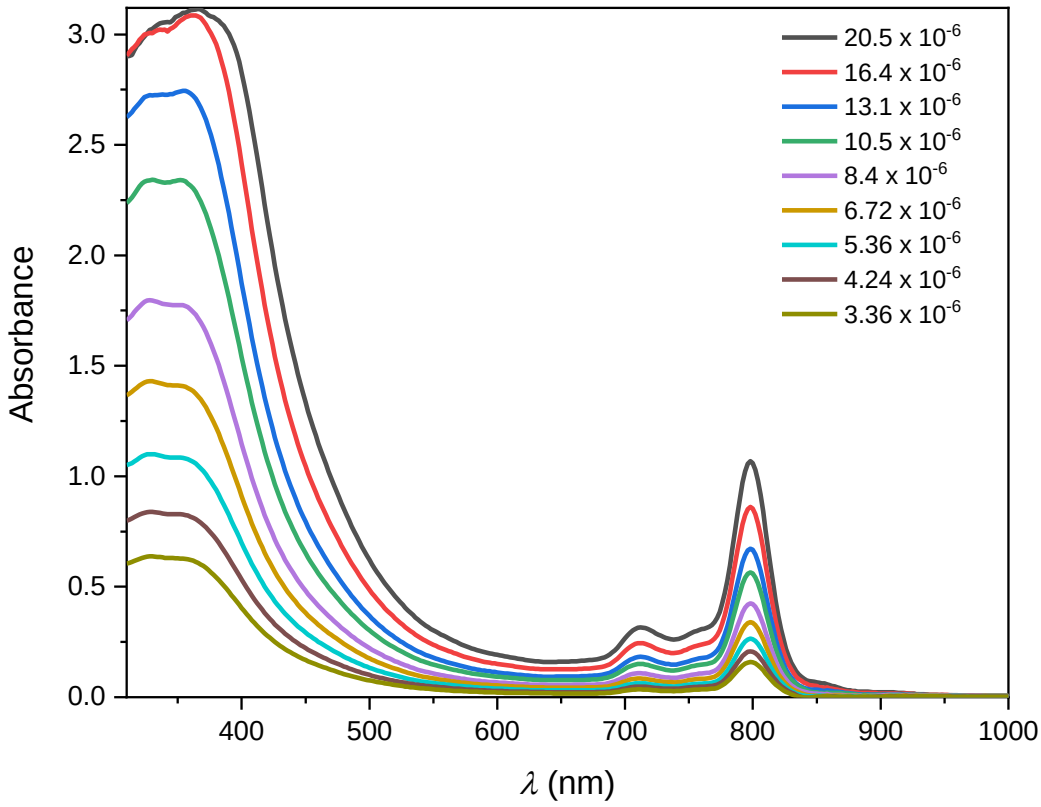


Fig. S38 UV-vis absorption spectra of **Zn-NMe$_2$Nc** in liquid DMSO at different concentrations.

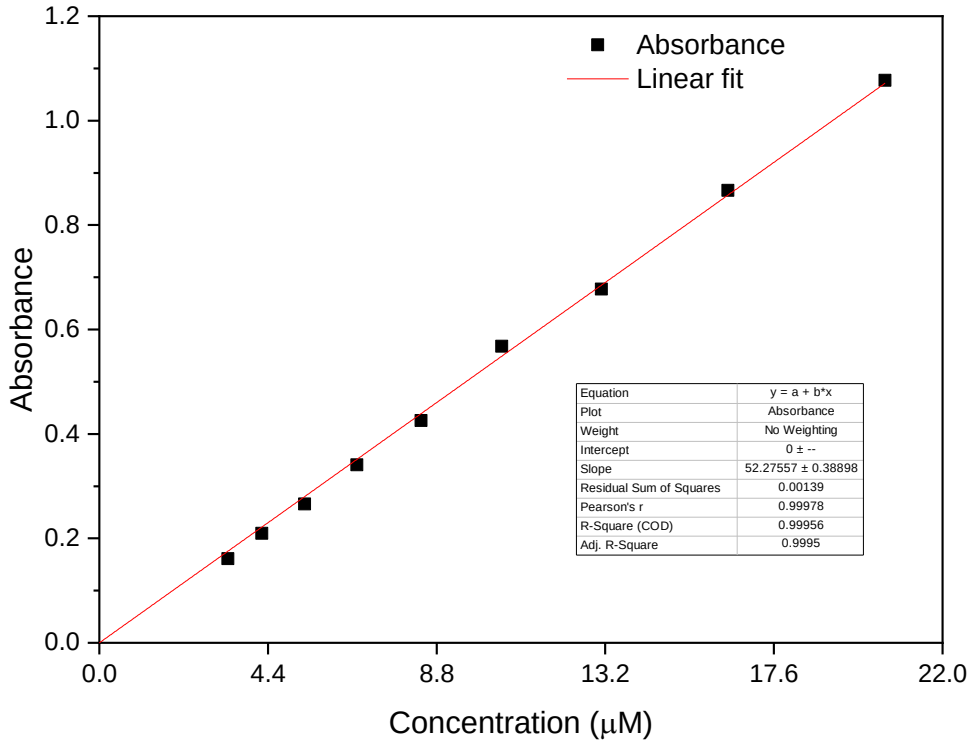


Fig. S39 Lambert-Beer law verified for **Zn-NMe$_2$Nc** in liquid DMSO at 298 K (λ_{max} = 800 nm).

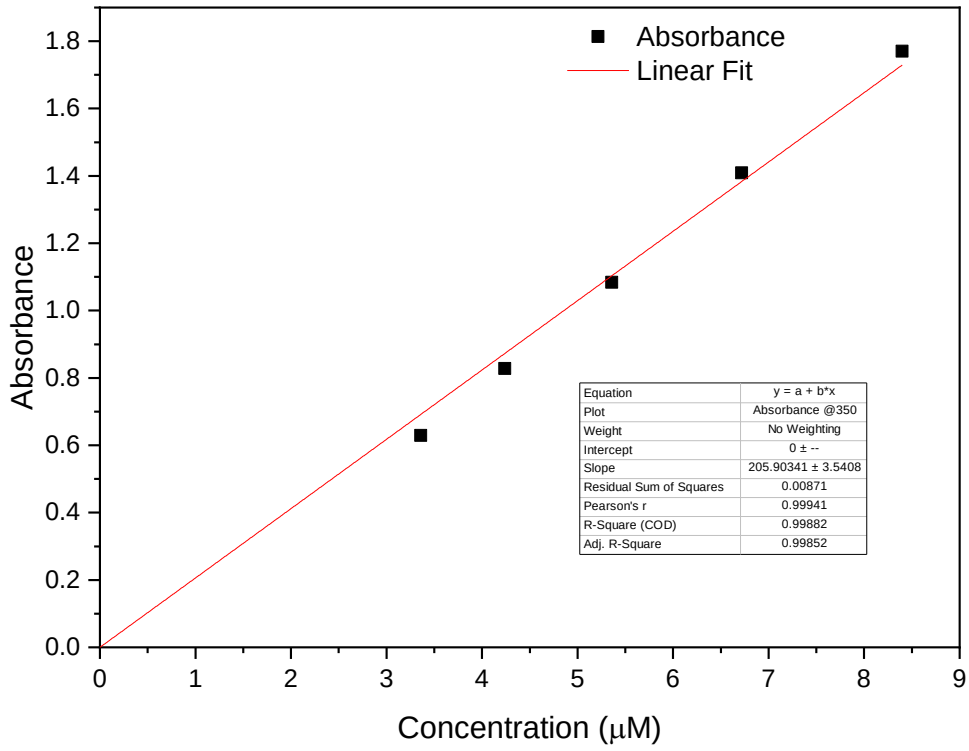


Fig. S40 Lambert-Beer law verified for **Zn-NMe$_2$Nc** in liquid DMSO at 298 K (λ_{max} = 350 nm).

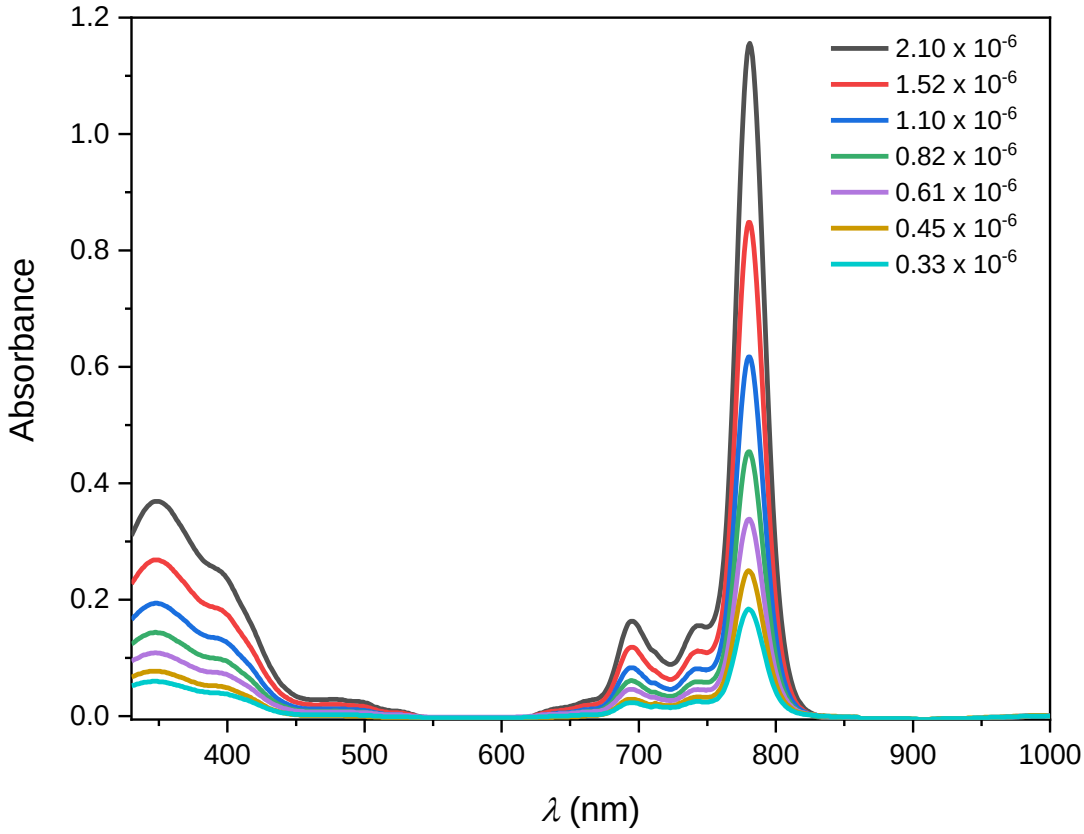


Fig. S41 UV-vis absorption spectra of **Zn-NMe$_3$Nc** in liquid DMSO at different concentrations.

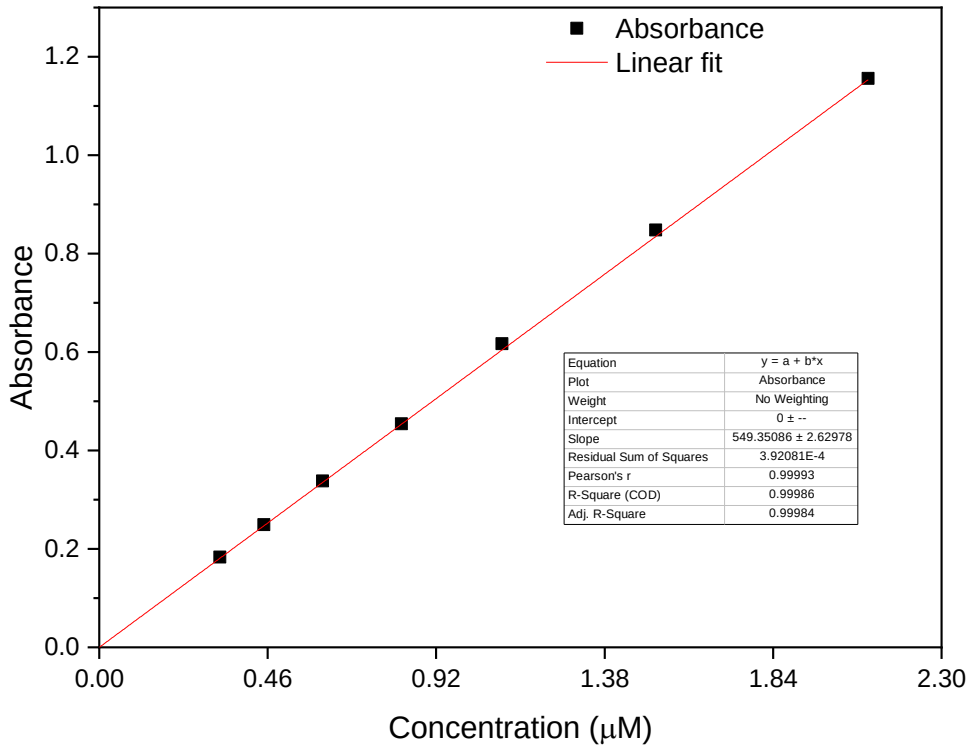


Fig. S42 Lambert-Beer law verified for **Zn-NMe$_3$Nc** liquid DMSO at 298 K (λ_{max} = 781 nm).

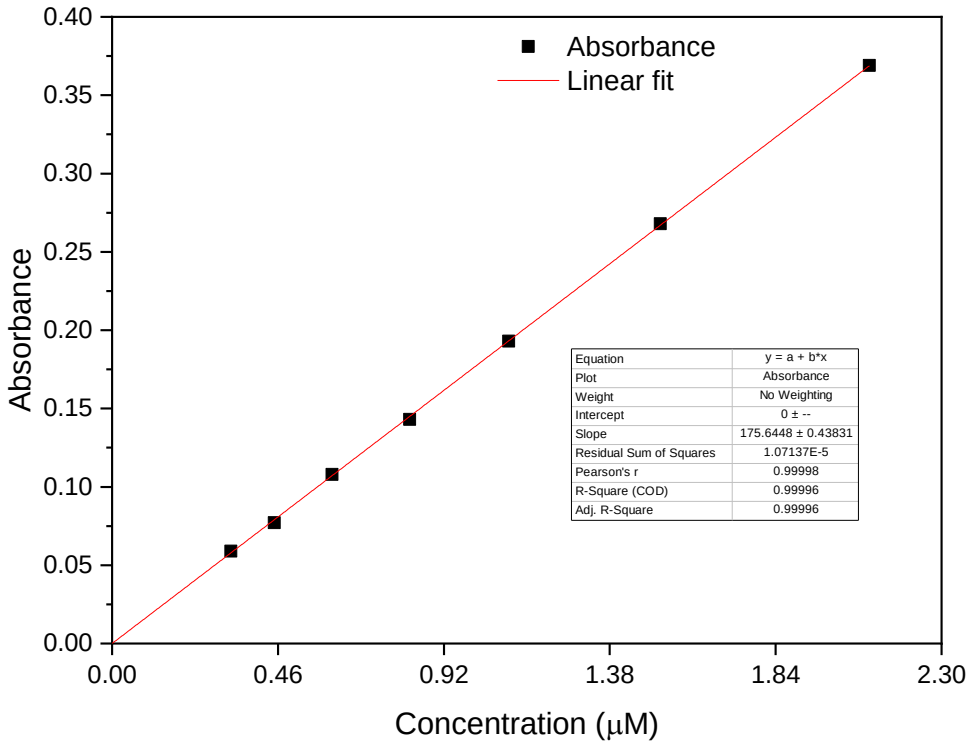


Fig. S43 Lambert-Beer law verified for **Zn-NMe$_3$Nc** liquid DMSO at 298 K (λ_{max} = 350 nm).

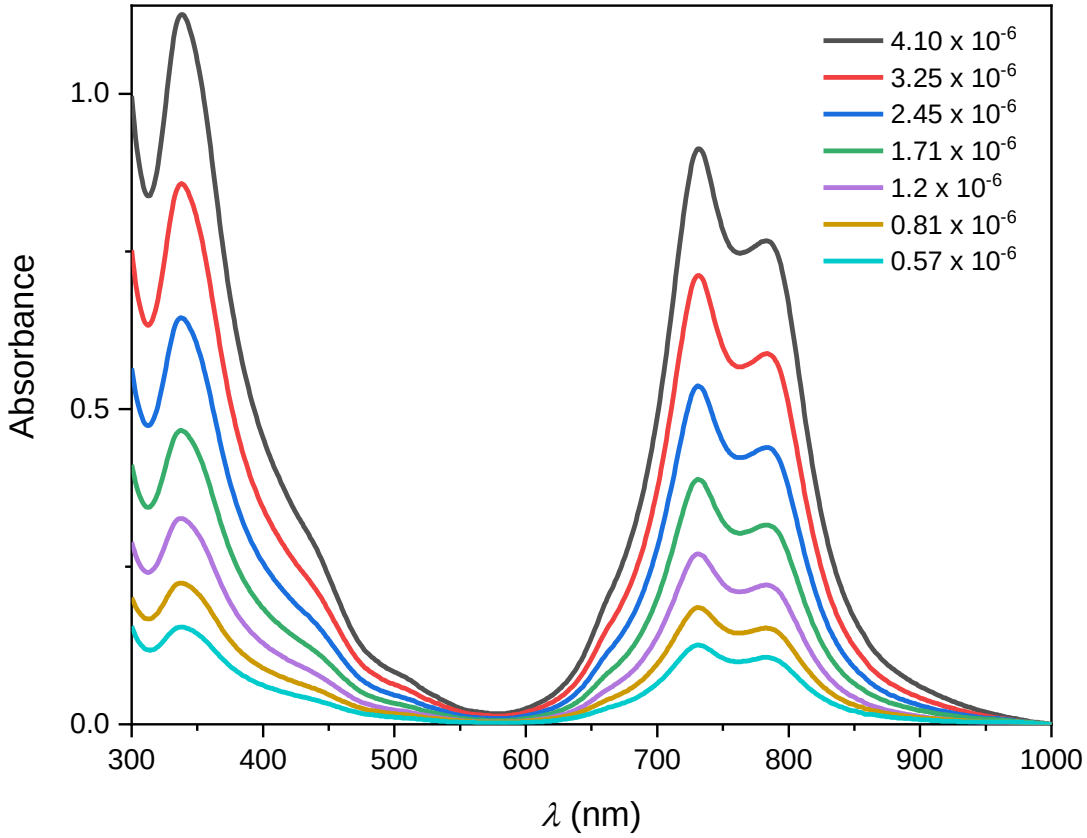


Fig. S44 UV-vis absorption spectra of **Zn-NMe$_3$Nc** in liquid water at different concentrations.

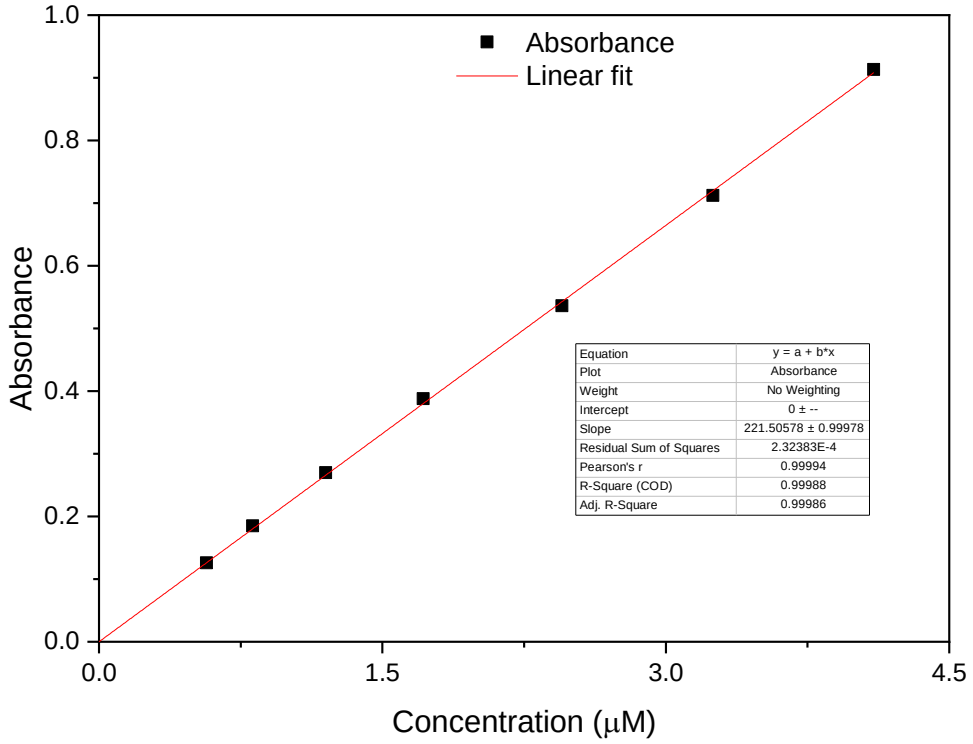


Fig. S45 Lambert-Beer law verified for **Zn-NMe$_3$Nc** in liquid water at 298 K (λ_{max} = 732 nm).

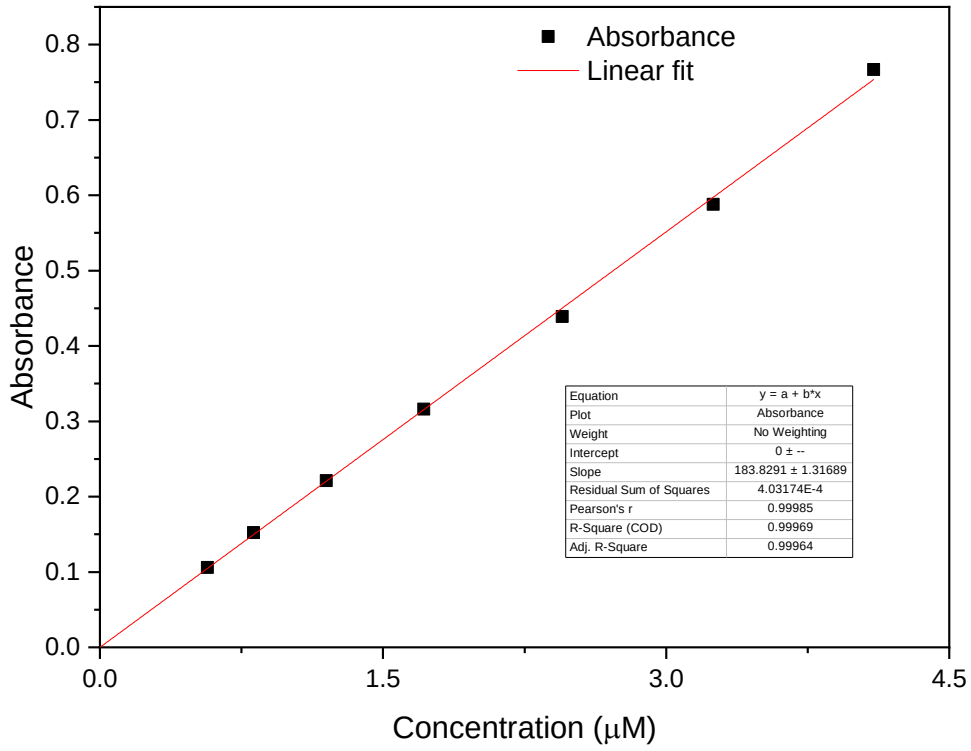


Fig. S46 Lambert-Beer law verified for **Zn-NMe$_3$Nc** in liquid water at 298 K (λ_{max} = 784 nm).

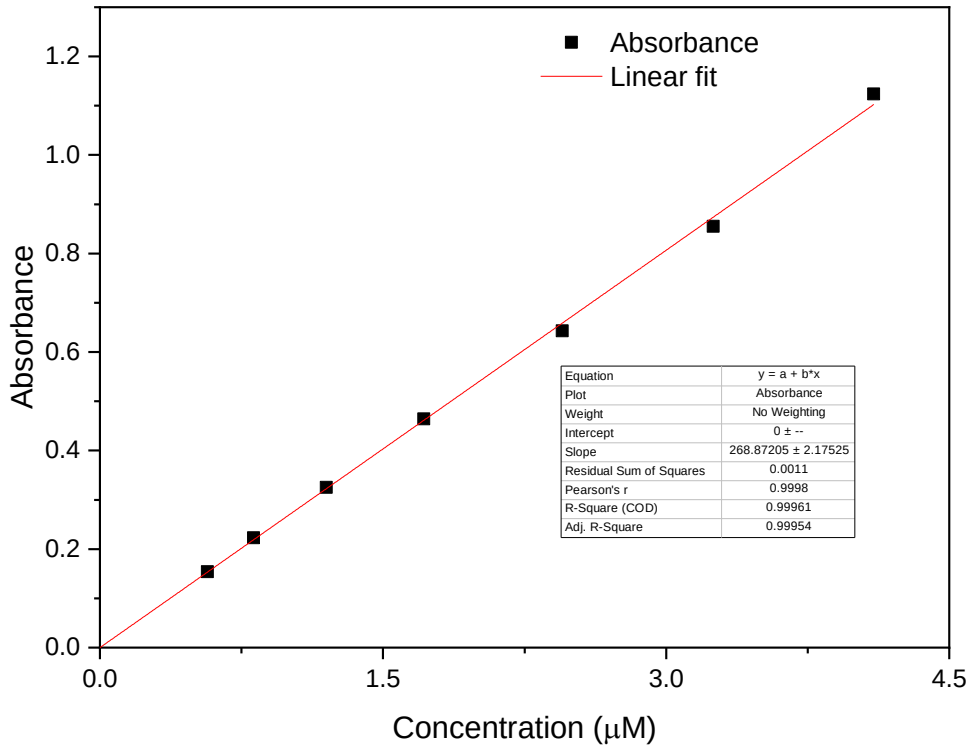
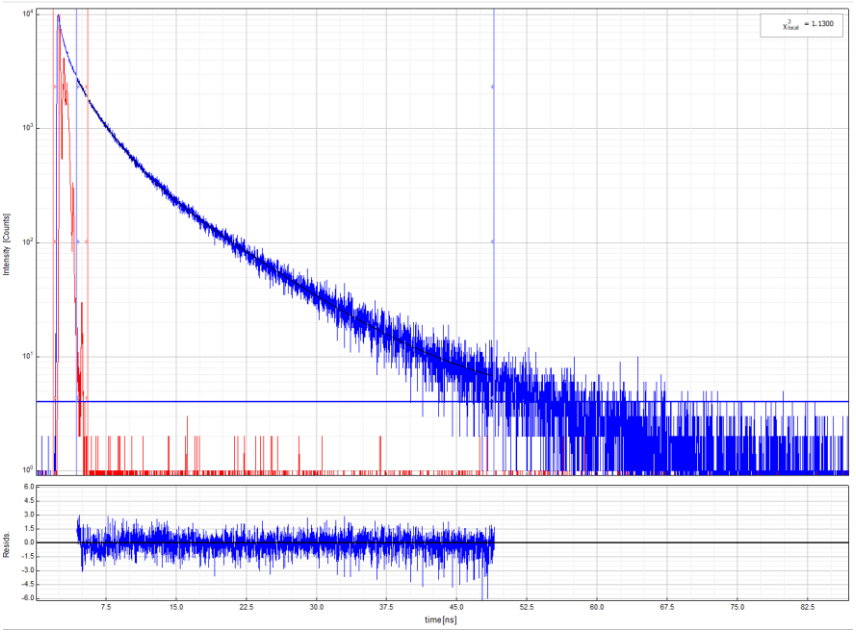
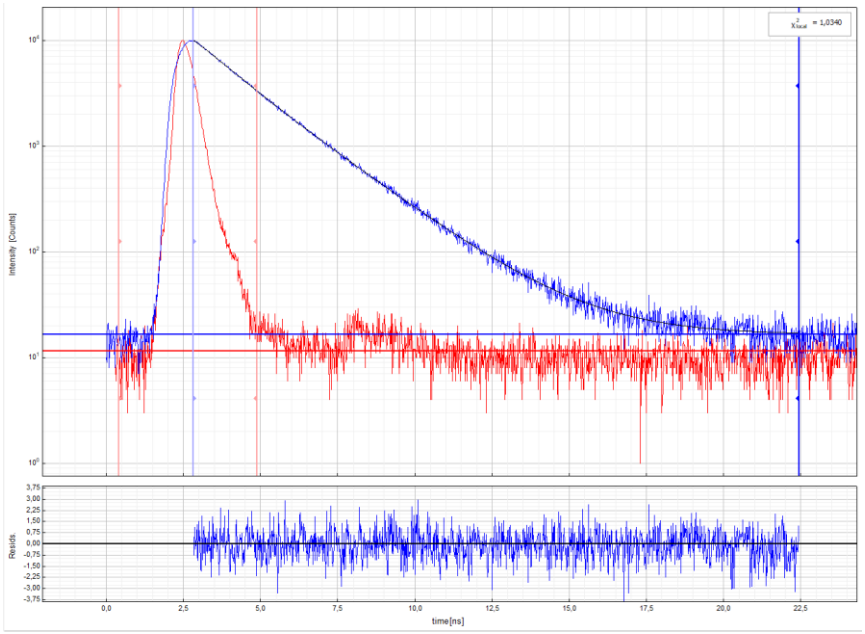


Fig. S47 Lambert-Beer law verified for **Zn-NMe$_3$Nc** in liquid water at 298 K (λ_{max} = 340 nm).



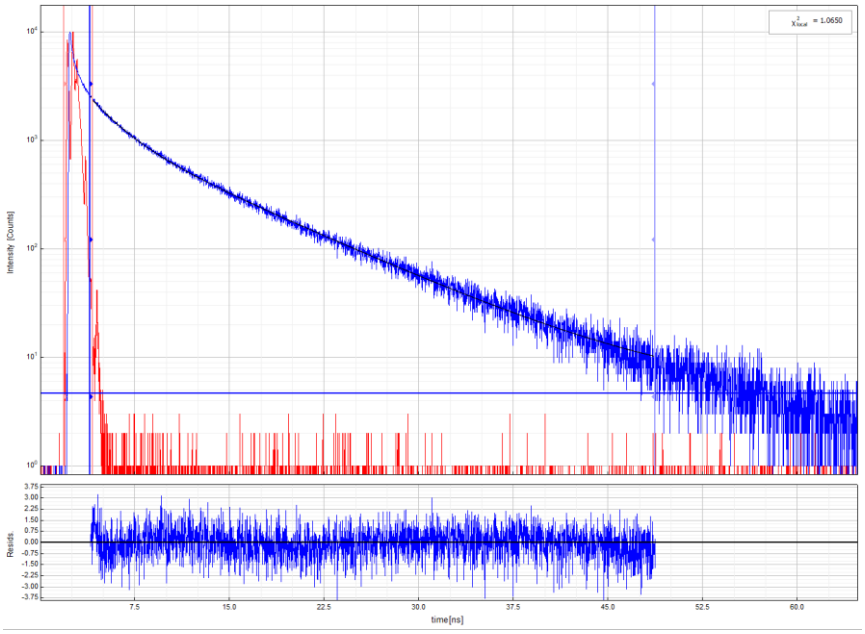
Parameter	Value	Error
A_1[kCnts/Chnl]	0.972	± 0.067
τ_1[ns]	8.15	± 0.25
I_1[kCnts]	495	± 22
$A_{Rel\,1}$[%]	20.9	± 1.3
$I_{Rel\,1}$[%]	44.4	± 1.9
A_2[kCnts/Chnl]	3.68	± 0.20
τ_2[ns]	2.69	± 0.11
I_2[kCnts]	619	± 40
$A_{Rel\,2}$[%]	79.1	± 1.3
$I_{Rel\,2}$[%]	55.6	± 1.9
$Bkgr_{Dec}$[kCnts]	0.0035	± 0.0006
$Bkgr_{IRF}$[Cnts/Chnl]	97	± 21
$Shift_{IRF}$[ps]	262	± 94
A_{Scatt}[kCnts]	-110	± 64
$\tau_{Av\,Int}$[ns]	5.119	± 0.091
$\tau_{Av\,Amp}$[ns]	3.833	± 0.093

Fig. S48 Left: Raw (experimental) time-resolved photoluminescence decay of **ZnOMeNc** in liquid DMSO (blue, c = 10^{-5} M) and the instrument response function (red) at 298 K, including the residuals (λ_{ex} = 376 nm, λ_{em} = 508 nm). Right: Fitting parameters including pre-exponential factors and confidence limits.



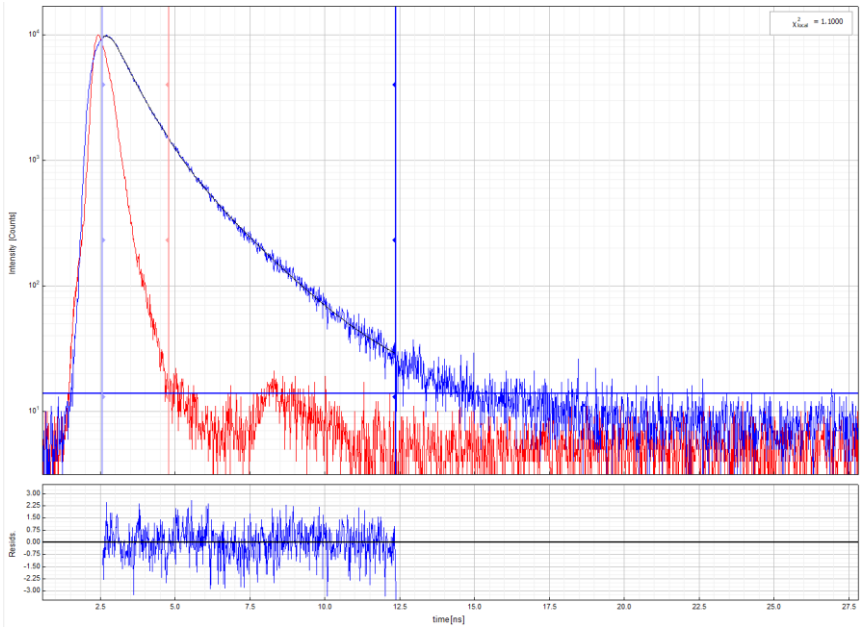
Parameter	Value	Error
A_1[kCnts/Chnl]	11,54	± 0,36
τ_1[ns]	2,052	± 0,025
I_1[kCnts]	1480	± 28
$A_{Rel\,1}$[%]	68,4	± 2,9
$I_{Rel\,1}$[%]	81,6	± 1,7
A_2[kCnts/Chnl]	5,32	± 0,74
τ_2[ns]	1,00	± 0,15
I_2[kCnts]	334	± 34
$A_{Rel\,2}$[%]	31,6	± 2,9
$I_{Rel\,2}$[%]	18,4	± 1,7
$Bkgr_{Dec}$[kCnts]	0,0164	± 0,0004
$Bkgr_{IRF}$[Cnts/Chnl]	5	± 23
$Shift_{IRF}$[ps]	-228	± 16
A_{Scatt}[kCnts]	-34	± 177
$\tau_{Av\,Int}$[ns]	1,859	± 0,039
$\tau_{Av\,Amp}$[ns]	1,721	± 0,085

Fig. S49 Left: Raw (experimental) time-resolved photoluminescence decay of **ZnOMeNc** in liquid DMSO (blue, c = 10^{-5} M) and the instrument response function (red) at 298 K, including the residuals (λ_{ex} = 376 nm, λ_{em} = 810 nm). Right: Fitting parameters including pre-exponential factors and confidence limits.



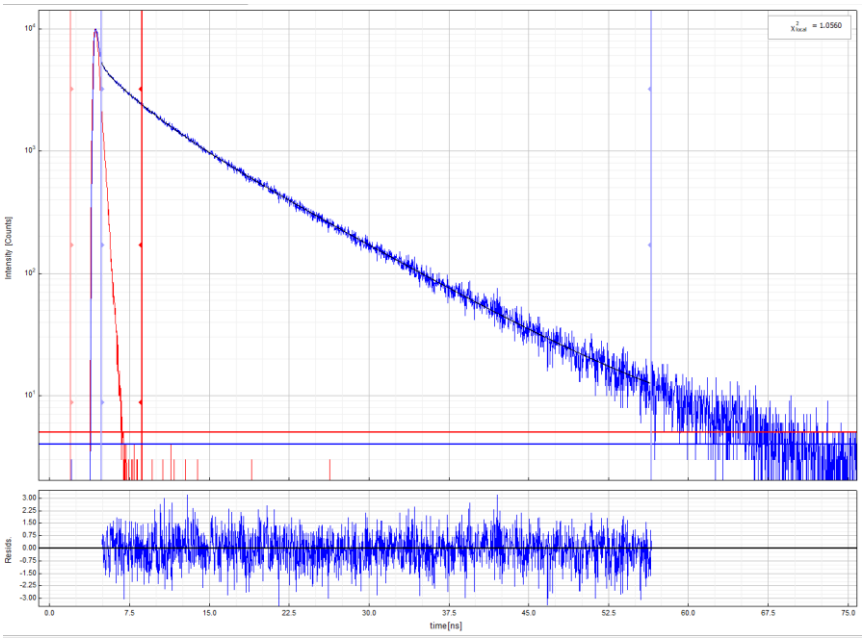
Parameter	Value	Error
A_1[kCnts/Chnl]	1.70	± 0.14
τ_1[ns]	8.37	± 0.18
I_1[kCnts]	888	± 77
$A_{Rel\,1}$[%]	38.73	± 0.90
$I_{Rel\,1}$[%]	70.0	± 1.6
A_2[kCnts/Chnl]	2.69	± 0.27
τ_2[ns]	2.27	± 0.15
I_2[kCnts]	381	± 43
$A_{Rel\,2}$[%]	61.27	± 0.90
$I_{Rel\,2}$[%]	30.0	± 1.6
$Bkgr_{Dec}$[kCnts]	0.0047	± 0.0006
$Bkgr_{IRF}$[Cnts/Chnl]	-201	± 188
$Shift_{IRF}$[ps]	-166	± 31
A_{Scatt}[kCnts]	118	± 365
$\tau_{Av\,Int}$[ns]	6.537	± 0.068
$\tau_{Av\,Amp}$[ns]	4.63	± 0.12

Fig. S50 Left: Raw (experimental) time-resolved photoluminescence decay of **Zn-NMe$_2$Nc** in liquid DMSO (blue, c = 10-5 M) and the instrument response function (red) at 298 K, including the residuals (λ_{ex} = 376 nm, λ_{em} = 560 nm). Right: Fitting parameters including pre-exponential factors and confidence limits.



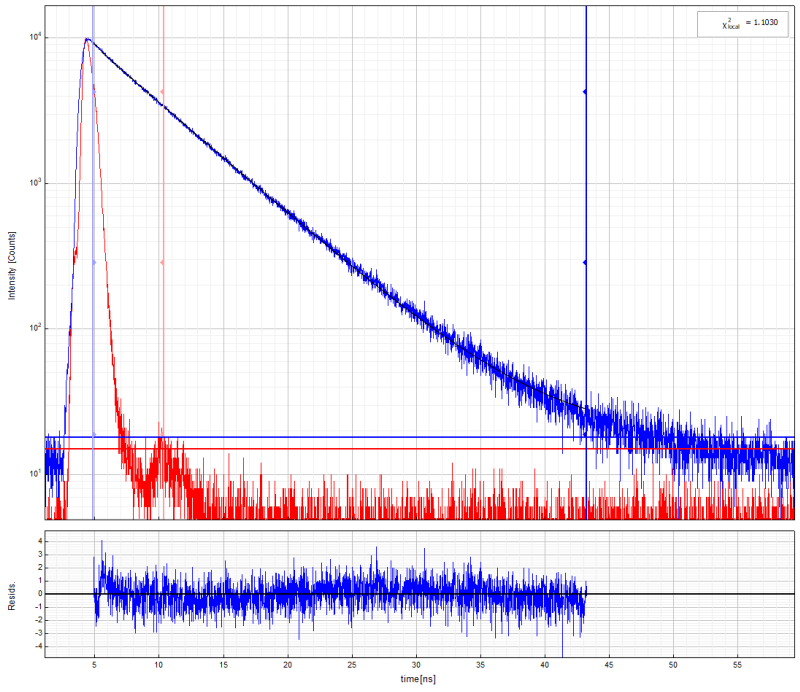
Parameter	Value	Error
A_1[kCnts/Chnl]	3.26	± 0.33
τ_1[ns]	1.801	± 0.083
I_1[kCnts]	367	± 22
$A_{Rel\,1}$[%]	21.0	± 2.0
$I_{Rel\,1}$[%]	43.8	± 2.4
A_2[kCnts/Chnl]	12.31	± 0.50
τ_2[ns]	0.614	± 0.032
I_2[kCnts]	472	± 18
$A_{Rel\,2}$[%]	79.0	± 2.0
$I_{Rel\,2}$[%]	56.2	± 2.4
$Bkgr_{Dec}$[kCnts]	0.0138	± 0.0046
$Bkgr_{IRF}$[Cnts/Chnl]	-40	± 43
$Shift_{IRF}$[ps]	250.0000	
A_{Scatt}[kCnts]	133	± 14
$\tau_{Av\,Int}$[ns]	1.133	± 0.027
$\tau_{Av\,Amp}$[ns]	0.863	± 0.038

Fig. S51 Left: Raw (experimental) time-resolved photoluminescence decay of **Zn-NMe$_2$Nc** in liquid DMSO (blue, c = 10^{-5} M) and the instrument response function (red) at 298 K, including the residuals (λ_{ex} = 376 nm, λ_{em} = 811 nm). Right: Fitting parameters including pre-exponential factors and confidence limits.



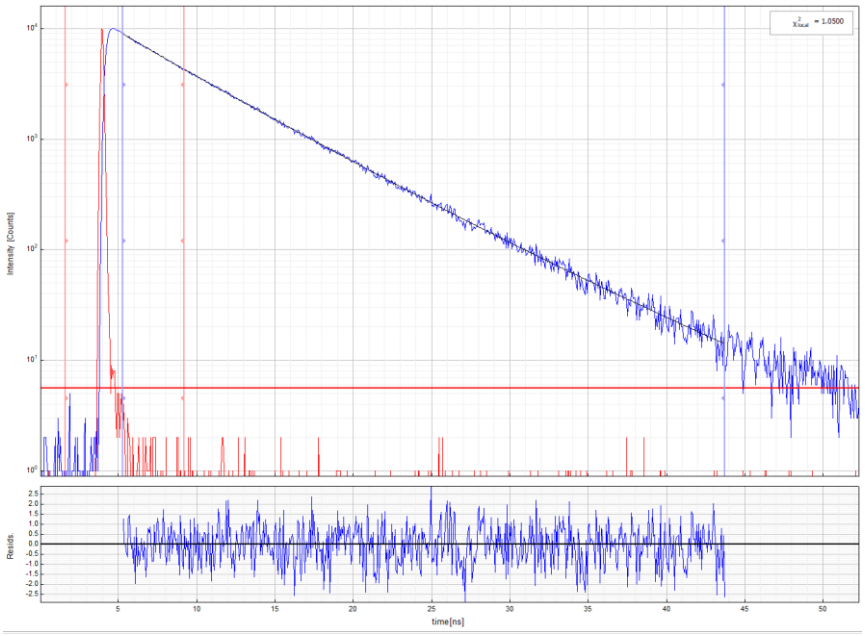
Parameter	Value	Error
A_1[kCnts/Chnl]	2.91	± 0.13
τ_1[ns]	9.06	± 0.21
I_1[kCnts]	824	± 20
$A_{Rel\,1}$[%]	55.4	± 2.7
$I_{Rel\,1}$[%]	76.7	± 3.0
A_2[kCnts/Chnl]	2.34	± 0.16
τ_2[ns]	3.42	± 0.42
I_2[kCnts]	250	± 40
$A_{Rel\,2}$[%]	44.6	± 2.7
$I_{Rel\,2}$[%]	23.3	± 3.0
$Bkgr_{Dec}$[kCnts]	0.0034	± 0.0010
$Bkgr_{IRF}$[Cnts/Chnl]	36	± 33
$Shift_{IRF}$[ps]	-32	± 37
A_{Scatt}[kCnts]	107	± 12
$\tau_{Av\,Int}$[ns]	7.748	± 0.062
$\tau_{Av\,Amp}$[ns]	6.55	± 0.20

Fig. S52 Left: Raw (experimental) time-resolved photoluminescence decay of **Zn-NMe$_3$Nc** in liquid DMSO (blue, c = 10^{-5} M) and the instrument response function (red) at 298 K, including the residuals (λ_{ex} = 376 nm, λ_{em} = 550 nm). Right: Fitting parameters including pre-exponential factors and confidence limits.



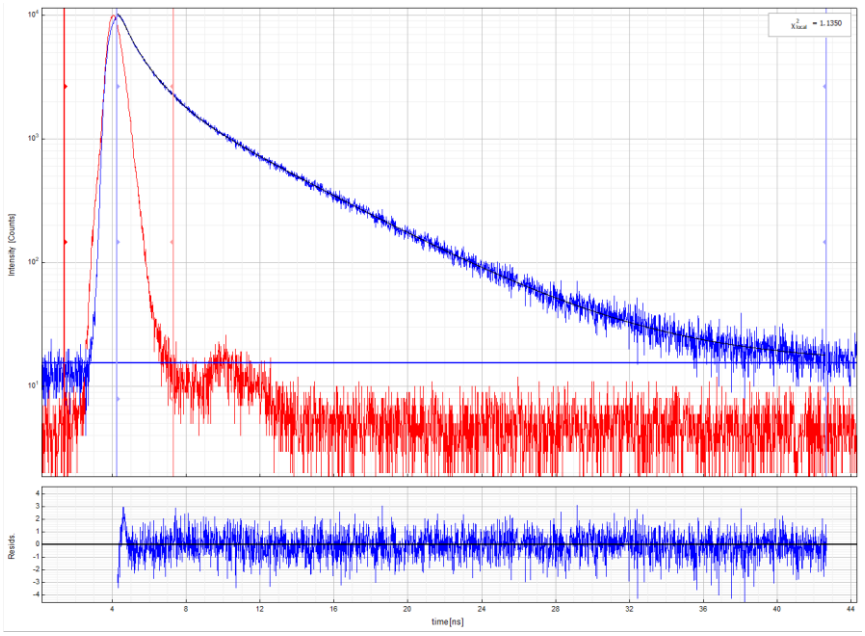
Parameter	Value	Error
A_1[kCnts/Chnl]	9.526	± 0.029
τ_1[ns]	5.689	± 0.016
I_1[kCnts]	3386.8	± 6.6
$A_{Rel\,1}$[%]	100.0000	± 0.0000
$I_{Rel\,1}$[%]	100.0000	± 0.0000
$Bkgr_{Dec}$[kCnts]	0.0148	± 0.0004
$Bkgr_{IRF}$[Cnts/Chnl]	15.0000	
$Shift_{IRF}$[ps]	500.0000	
A_{Scatt}[kCnts]	272.6	± 9.2
$\tau_{Av\,Int}$[ns]	5.689	± 0.016
$\tau_{Av\,Amp}$[ns]	5.689	± 0.016

Fig. S53 Left: Raw (experimental) time-resolved photoluminescence decay of **Zn-NMe$_3$Nc** in liquid DMSO (blue, c = 10^{-5} M) and the instrument response function (red) at 298 K, including the residuals (λ_{ex} = 376 nm, λ_{em} = 801 nm). Right: Fitting parameters including pre-exponential factors and confidence limits.



Parameter	Value	Error
A_1[kCnts/Chnl]	1.06	± 0.15
τ_1[ns]	8.49	± 0.44
I_1[kCnts]	140	± 17
$A_{Rel\,1}$[%]	9.1	± 1.2
$I_{Rel\,1}$[%]	14.1	± 1.7
A_2[kCnts/Chnl]	10.53	± 0.20
τ_2[ns]	5.209	± 0.070
I_2[kCnts]	857	± 24
$A_{Rel\,2}$[%]	90.9	± 1.2
$I_{Rel\,2}$[%]	85.9	± 1.7
$Bkgr_{Dec}$[kCnts]	-0.0003	± 0.0020
$Bkgr_{IRF}$[Cnts/Chnl]	5.6	± 2.6
$Shift_{IRF}$[ps]	-162	± 34
A_{Scatt}[kCnts]	203	± 208
$\tau_{Av\,Int}$[ns]	5.670	± 0.023
$\tau_{Av\,Amp}$[ns]	5.508	± 0.030

Fig. S54 Left: Raw (experimental) time-resolved photoluminescence decay of **Zn-NMe$_3$Nc** in liquid H_2O (blue, c = 10^{-5} M) and the instrument response function (red) at 298 K, including the residuals (λ_{ex} = 376 nm, λ_{em} = 432 nm). Right: Fitting parameters including pre-exponential factors and confidence limits.



Parameter	Value	Error
A_1[kCnts/Chnl]	2.919	± 0.060
τ_1[ns]	5.432	± 0.051
I_1[kCnts]	991	± 19
$A_{Rel\,1}$[%]	28.5	± 1.2
$I_{Rel\,1}$[%]	64.5	± 1.2
A_2[kCnts/Chnl]	7.32	± 0.51
τ_2[ns]	1.192	± 0.079
I_2[kCnts]	546	± 37
$A_{Rel\,2}$[%]	71.5	± 1.2
$I_{Rel\,2}$[%]	35.5	± 1.2
$Bkgr_{Dec}$[kCnts]	0.0154	± 0.0006
$Bkgr_{IRF}$[Cnts/Chnl]	-10	± 33
$Shift_{IRF}$[ps]	91	± 66
A_{Scatt}[kCnts]	355	± 22
$\tau_{Av\,Int}$[ns]	3.927	± 0.054
$\tau_{Av\,Amp}$[ns]	2.40	± 0.12

Fig. S55 Left: Raw (experimental) time-resolved photoluminescence decay of **Zn-NMe$_3$Nc** in liquid H_2O (blue, c = 10^{-5} M) and the instrument response function (red) at 298 K, including the residuals (λ_{ex} = 376 nm, λ_{em} = 804 nm). Right: Fitting parameters including pre-exponential factors and confidence limits.

Section S4: DFT calculations

Table S1. Monomer emission wavelengths (in nm) for the $S_1 \rightarrow S_0$ and $S_3 \rightarrow S_0$ transitions as obtained from the difference in energy between the corresponding optimized singlet geometries obtained with CAM-B3LYP functional.

	Zn-NMe$_2$Nc (λ_{max} / nm)	**Zn-OMeNc (λ_{max} / nm)**	**Zn-NMe$_3$Nc (λ_{max} / nm)**
S_1 (0-0)	839.40	828.20	817.60
S_1 (vertical)	888.20	874.90	861.70
S_3 (0-0)	450.50	390.40	393.90
S_3 (vertical)	503.00	397.10	392.90

Table S2. Monomer emission wavelengths (in nm) for the $S_1 \rightarrow S_0$ and $S_3 \rightarrow S_0$ transitions as obtained from the difference in energy between the corresponding optimized singlet geometries obtained with M06-2X functional.

	Zn-NMe$_2$Nc (λ_{max} / nm)	**Zn-OMeNc (λ_{max} / nm)**	**Zn-NMe$_3$Nc (λ_{max} / nm)**
S_1 (0-0)	816.60	802.90	792.80
S_1 (vertical)	888.20	874.90	861.70
S_3 (0-0)	479.40	393.70	397.80
S_3 (vertical)	503.40	397.10	392.90

Table S3. TDDFT output for the optimized S_1 state with the PBE0 functional.

Zn-NMe$_2$Nc:

Excited State 1: Singlet 1.3859 eV 894.60 nm f=1.5426 <S**2>=0.000
450 -> 451 -0.70315

Excited State 2: Singlet 1.5712 eV 789.13 nm f=1.3333 <S**2>=0.000
450 -> 452 -0.69721

Excited State 3: Singlet 1.7517 eV 707.81 nm f=0.0100 <S**2>=0.000
446 -> 451 0.62707
447 -> 451 -0.29216
448 -> 451 -0.11923

Zn-OMeNc:

Excited State 1: Singlet 1.4583 eV 850.21 nm f=1.4799 <S**2>=0.000
418 -> 419 0.70495

Excited State 2: Singlet 1.6333 eV 759.12 nm f=1.3475 <S**2>=0.000
418 -> 420 0.70296

Excited State 3: Singlet 2.5219 eV 491.63 nm f=0.0012 <S**2>=0.000
416 -> 419 -0.63757
417 -> 419 0.26909

Zn-Nme$_3$Nc:

Excited State 1: Singlet 1.4946 eV 829.57 nm f=1.4806 <S**2>=0.000
482 -> 483 0.70479

Excited State 2: Singlet 1.6640 eV 745.10 nm f=1.3553 <S**2>=0.000
482 -> 484 -0.70290

Excited State 3: Singlet 2.6522 eV 467.48 nm f=0.0001 <S**2>=0.000
482 -> 485 0.70323

Table S4. TDDFT output for the optimized S_3 state with the PBE0 functional.

Zn-NMe$_2$Nc:

Excited State 1: Singlet 1.3854 eV 894.91 nm f=1.5975 <S**2>=0.000
450 -> 451 0.70308

Excited State 2: Singlet 1.5737 eV 787.86 nm f=1.1410 <S**2>=0.000
449 -> 451 0.18743
450 -> 452 0.67370

Excited State 3: Singlet 1.6277 eV 761.73 nm f=0.2369 <S**2>=0.000
449 -> 451 0.67946
450 -> 452 -0.18547

Excited State 4: Singlet 1.7639 eV 702.90 nm f=0.0656 <S**2>=0.000
446 -> 451 -0.70249

Excited State 5: Singlet 1.7858 eV 694.26 nm f=0.1647 <S**2>=0.000
448 -> 451 -0.70360

Zn-OMeNc:

Excited State 1: Singlet 1.4392 eV 861.48 nm f=1.4669 <S**2>=0.000
418 -> 419 0.70502
Excited State 2: Singlet 1.6550 eV 749.15 nm f=1.4042 <S**2>=0.000
418 -> 420 0.70253

Excited State 3: Singlet 2.2385 eV 553.88 nm f=0.1551 <S**2>=0.000
417 -> 419 0.70275

Excited State 4: Singlet 2.4568 eV 504.66 nm f=0.1417 <S**2>=0.000
413 -> 419 0.18122
417 -> 420 0.67214

Excited State 5: Singlet 2.5027 eV 495.39 nm f=0.1582 <S**2>=0.000
413 -> 419 0.62512
415 -> 419 -0.18271
416 -> 419 0.17749
417 -> 420 -0.16789

Zn-Nme$_3$Nc:

Excited State 1: Singlet 1.5755 eV 786.93 nm f=1.4257 <S**2>=0.000
482 -> 483 -0.70393

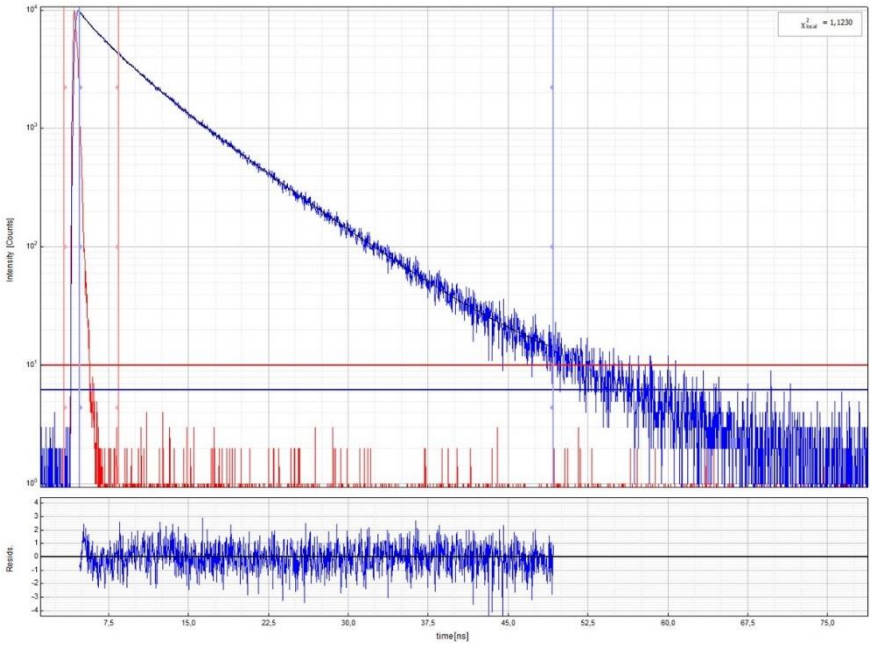
Excited State 2: Singlet 1.5781 eV 785.66 nm f=1.4059 <S**2>=0.000
482 -> 484 -0.70393

Excited State 3: Singlet 2.6031 eV 476.29 nm f=0.0002 <S**2>=0.000
482 -> 485 0.70369

Excited State 4: Singlet 2.7217 eV 455.54 nm f=0.0002 <S**2>=0.000
482 -> 486 -0.70132

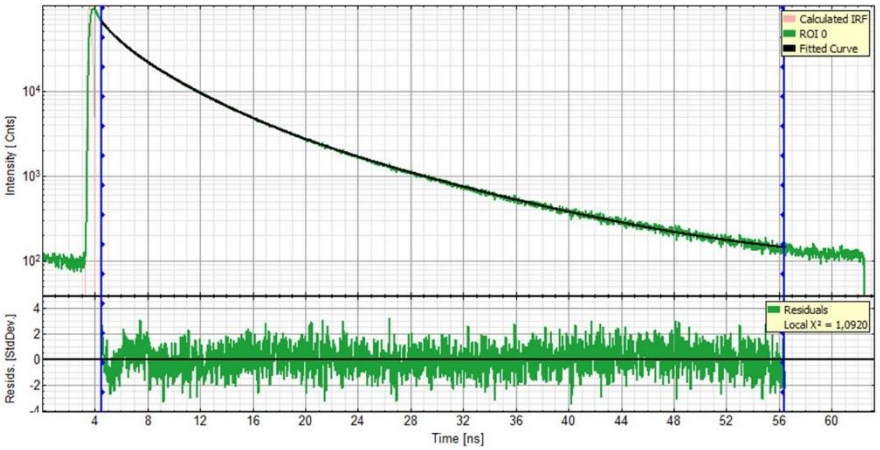
Excited State 5: Singlet 2.7975 eV 443.20 nm f=0.1784 <S**2>=0.000
482 -> 487 0.70167

Section S5: ZnNMe$_2$Nc loaded onto polystyrene microparticles (PSMPs)



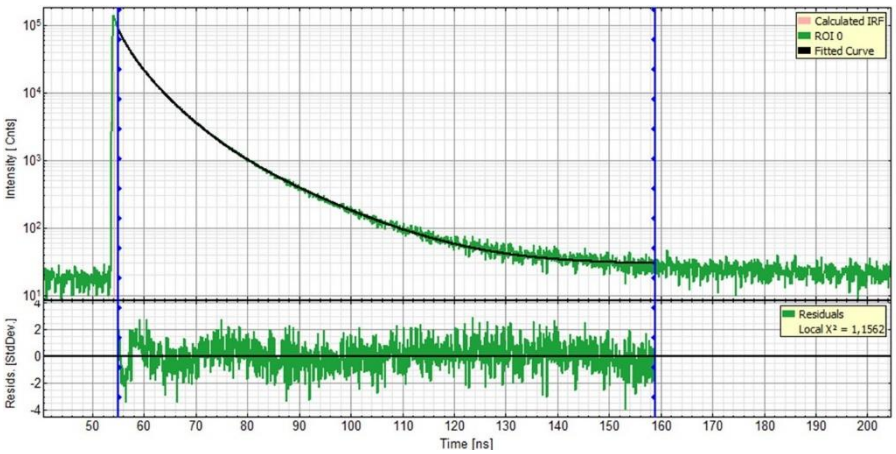
Parameter	Value	Error
A_1[kCnts/Chnl]	5,84	± 0,31
τ_1[ns]	6,81	± 0,12
I_1[kCnts]	1244	± 46
$A_{Rel\,1}$[%]	56,2	± 2,7
$I_{Rel\,1}$[%]	75,0	± 2,7
A_2[kCnts/Chnl]	4,55	± 0,25
τ_2[ns]	2,91	± 0,15
I_2[kCnts]	414	± 44
$A_{Rel\,2}$[%]	43,8	± 2,7
$I_{Rel\,2}$[%]	25,0	± 2,7
$Bkgr_{Dec}$[kCnts]	0,0063	± 0,0012
$Bkgr_{IRF}$[Cnts/Chnl]	10,0000	
$Shift_{IRF}$[ps]	-6,0047	
A_{Scatt}[kCnts]	95,3	± 8,8
$\tau_{Av\,Int}$[ns]	5,839	± 0,021
$\tau_{Av\,Amp}$[ns]	5,105	± 0,033

Figure S56 Left: Raw (experimental) time-resolved photoluminescence decay of **ZnNMe$_2$Nc@PSMP** in H_2O (blue) and the instrument response function (red) at 298 K, including the residuals (λ_{ex} = 376 nm, λ_{em} = 475 nm). Right: Fitting parameters including pre-exponential factors and confidence limits.



Parameter		Data Set (3)
τ_1 [ns]	Limits	10,100 ± 0,073
τ_2 [ns]	Limits	3,670 ± 0,031
τ_3 [ns]	Limits	1,090 ± 0,024
$Bkgr_{Dec}$[Cnts]	Limits	88,0 ± 2,4
I_1 [kCnts]		4911 ± 47
I_2 [kCnts]		6814 ± 69
I_3 [kCnts]		1032 ± 35
I_{Sum}[kCnts]		12757,0 ± 8,8
A_{Sum}[kCnts]		66,00 ± 0,15
$\tau_{Av\,Int}$[ns]		5,950 ± 0,019
$\tau_{Av\,Amp}$[ns]		3,870 ± 0,011
$A_{rel\,1}$		0,147 ± 0,002
$A_{rel\,2}$		0,564 ± 0,004
$A_{rel\,3}$		0,2889 ± 0,0036

Figure S57 Left: Raw (experimental) time-resolved photoluminescence decay of **ZnNMe$_2$Nc@PSMP** observed under the confocal microscope (SPE) and the instrument response function (red) at 298 K, including the residuals (λ_{ex} = 376 nm, 460 LP filter). Right: Fitting parameters including pre-exponential factors and confidence limits.



Parameter		Overall Decay
t_0[ns]		54,8800 ± ------
A_1 [kCnts]	Limits	48,00 ± 0,25
A_2 [kCnts]	Limits	6,600 ± 0,078
A_3 [kCnts]	Limits	39,00 ± 0,19
τ_1 [ns]	Limits	4,630 ± 0,016
τ_2 [ns]	Limits	12,000 ± 0,052
τ_3 [ns]	Limits	1,720 ± 0,031
$Bkgr_{Dec}$ [Cnts]	Limits	65 ± 1
I_1 [kCnts]		2798,0 ± 8,2
I_2 [kCnts]		992,0 ± 8,3
I_3 [kCnts]		835 ± 16
I_{Sum} [kCnts]		4625,0 ± 1,9
A_{Sum} [kCnts]		94,00 ± 0,13
$\tau_{Av Int}$ [ns]		5,6920 ± 0,0034
$\tau_{Av Amp}$ [ns]		3,9430 ± 0,0065

Figure S58 Left: Raw (experimental) time-resolved photoluminescence decay of **Zn-NMe$_2$Nc@PSNP** observed under the confocal microscope (TPE) and the instrument response function (red) at 298 K, including the residuals (λ_{ex} = 810 nm, 460 LP filter). Right: Fitting parameters including pre-exponential factors and confidence limits.